DEVELOPMENT OF SOLID ACID CATALYSTS FOR CELLULOSE ACETATE PRODUCTION

A Thesis Submitted to
the Graduate School of Engineering and Sciences of
İzmir Institute of Technology
in Partial Fulfillment of the Requirements for the Degree of

MASTER OF SCIENCE

in Chemical Engineering

by
Begüm SÖNMEZTÜRK

June 2022

İZMİR

ACKNOWLEDGMENTS

I would like to express my gratitude to my advisor Prof. Selahattin Yılmaz for his continuous support and effort during my graduate studies. He has always mentored me to develop a better perspective and kept me motivated about my research with his sincerity and kindness.

I would like to thank my dear friends, Azime Arıkaya, Günsev Dizoğlu, Tuğçe Özperçin, and Mustafa Kalkandelen for their kindness and support during my thesis. I also would like to thank Ahmet Kurul, Nazil Karaca, Belgin Tunçel Kırkar, Ali Oğuz Büyükkileci, Hüseyin Özgener, IYTE CMR, and Environmental R&D for their assistance.

My special thanks go to my dear husband Osman Sönmeztürk and my parents for their endless support and continuous encouragement throughout my thesis.

ABSTRACT

DEVELOPMENT OF SOLID ACID CATALYSTS FOR CELLULOSE ACETATE PRODUCTION

Cellulose acetate (CA) is one of the most commercially important cellulose derivatives with a wide range of applications in various industries. As a green approach, the development of heterogeneous solid acid catalysts for cellulose acetate production is important. The objective of the present thesis is to develop active and stable mesoporous solid acid catalysts for solventless cellulose acetate production with acetic anhydride from microcrystalline cellulose. As catalyst sulfating agents, ammonium sulfate and chlorosulfonic acid (CSA) were applied. Ammonium sulfate ($(NH_4)_2SO_4$) sulfated catalysts are La incorporated titania-silica ($SO_4/La\text{-}TiO_2\text{-}SiO_2$), sulfated titania-silica ($SO_4/TiO_2\text{-}SiO_2$), and sulfated Ti-SBA-15 (SO_4/Ti-SBA-15), whereas the CSA/Ti-SBA-15 catalysts were sulfated by chlorosulfonic acid. The effect of Si/Ti mole ratios (6, 10, 20) on the stability of CSA/Ti-SBA-15 catalysts was investigated.

Activity and stability of the catalysts were tested in the cellulose acetylation reaction by acetic anhydride at 80 ^oC with a 10:1 acetic anhydride to cellulose AGU mole ratio. The effect of reaction time (2, 4, 6, and 8 h) and amount of catalyst (0.10, 0.25, and 0.5 g) on the reaction were investigated. Synthesized cellulose acetate samples were analyzed by FT-IR, ^{1}H-NMR, and TGA. CSA/Ti-SBA-15 (10) was found to be the most active and stable catalyst with 2.84 % leaching, 89.6 % conversion, 74.6 % yield, and DS of 2.69. The activity and stability of CSA/Ti-SBA-15 (10) catalyst were further investigated after its treatment with acetone. At the end of the 3rd cycle, A-CSA/Ti-SBA-15 (10) was found as an active and stable catalyst with 58.6% cellulose conversion, 50% CA yield, DS of 2.62, and 1.68% sulfur leaching.

ÖZET

SELÜLOZ ASETAT ÜRETİMİ İÇİN KATI ASİT KATALİZÖRLERİNİN GELİŞTİRİLMESİ

Selüloz asetat (CA), çeşitli endüstrilerde geniş bir uygulama yelpazesine sahip ticari olarak en önemli selüloz türevlerinden biridir. Yeşil bir yaklaşım olarak, selüloz asetat üretimi için heterojen katı asit katalizörlerinin geliştirilmesi önemlidir. Bu tezin amacı, mikrokristalin selülozdan asetik anhidrit ile solventsiz selüloz asetat üretimi için aktif ve kararlı heterojen katı asit katalizörleri geliştirmektir. Katalizör sülfatlama kaynağı olarak amonyum sülfat ve klorosülfonik asit (CSA) kullanılmıştır. Amonyum sülfat ($(NH_4)_2SO_4$) ile sülfatlanmış katalizörler, La dahil edilmiş titanya-silika (SO_4/La-TiO_2-SiO_2), sülfatlanmış titanya-silika (SO_4/TiO_2-SiO_2) ve sülfatlanmış Ti-SBA-15'tir (SO4/Ti-SBA-15). CSA/Ti-SBA-15 katalizörleri ise klorosülfonik asit ile sülfatlanmıştır. Si/Ti mol oranlarının (6, 10, 20) CSA/Ti-SBA-15 katalizörlerinin stabilitesi üzerindeki etkisi araştırılmıştır.

Katalizörlerin aktivitesi ve stabilitesi, 10:1 asetik anhidrit/selüloz AGU mol oranı ile 80 °C'de asetik anhidrit ile selüloz asetilasyon reaksiyonunda test edilmiştir. Reaksiyon süresinin (2, 4, 6 ve 8 saat) ve katalizör miktarının (0.10, 0.25 ve 0.5 g) reaksiyon üzerindeki etkisi araştırılmıştır. Sentezlenen selüloz asetat numuneleri FT-IR, ^{1}H-NMR ve TGA ile analiz edilmiştir. CSA/Ti-SBA-15 (10) katalizörü, %2.84 liç, %89.6 dönüşüm, %74.6 verim ve 2.69 DS ile en aktif ve kararlı katalizör olarak bulunmuştur. CSA/Ti-SBA-15 (10) katalizörünün aktivitesi ve stabilitesi aseton ile muamele edildikten sonra da araştırılmıştır. 3. reaksiyon döngüsü sonunda A-CSA/Ti-SBA-15 (10) katalizörünün %58.6 selüloz dönüşümü, %50 CA verimi, 2.62 DS ve %1.68 kükürt liçi ile aktif ve kararlı bir katalizör olduğu bulunmuştur.

TABLE OF CONTENTS

LIST OF FIGURES

Figure **Page**

Figure **Page**

LIST OF TABLES

Table **Page**

Table **Page**

CHAPTER 1

INTRODUCTION

There is an increasing worldwide interest in biomass as a feedstock, due to the depletion of petroleum-based resources, environmental pollution problems, stringent environmental requirements on waste disposal, and the search for renewable resources. Since the 1980s, there has been a tremendous increase in research and development studies related to cellulose as a biobased raw material to produce environmentally friendly, high-performance polymeric products and value-added chemicals [1].

Cellulose is one of the most abundant, renewable, and biodegradable polymers, with an estimated annual production of 150 billion tons. Main cellulose sources are cotton linters and wood pulp. Cellulose is a significant raw material to produce essential chemicals, different paper products, as well as many other industrial products [2,3].

One of the significant classes of chemical intermediates is organic esters, which are commonly used in fine chemicals, cosmetics, medicines, and surfactants [4]. Cellulose acetate (CA) is one of the most commercially important cellulose ester derivatives with a wide range of applications in various industries due to its high mechanical strength, and non-toxic and biodegradable nature. It is produced from the acetylation of cellulose hydroxyl groups with an acetylation reagent. This substitution reaction is known as esterification, which is an exothermic equilibrium reaction taking place between acetic anhydride (Ac_2O) and the hydroxyl (OH) groups of cellulose.

Compared to cellulose, microcrystalline cellulose (MCC) is a more economical raw material for cellulose acetylation. However, the degree of polymerization (DP) (which is the number of anhydroglucose units, AGU) of technically available cellulose varies from 100 to 3000. A high DP decreases the reactivity of the cellulose because depending on the chain length of the cellulose, the hydroxyl groups may possess different accessibility for reagents [5]. MCC has a lower DP than cellulose (~300) as a reactant, so it is more suitable as a raw material for cellulose esterification.

Industrial cellulose acetate production has been carried out catalytically homogeneous by reacting cellulose with acetic anhydride in the presence of acetic acid and strong mineral acids, such as sulfuric acid or perchloric acid as the catalyst [6]. Mineral acids possess good catalytic activity, however, product separation, purification, and hard reuse lead to high production costs. It has also been reported that the utilization of strong inorganic acid catalysts results in issues such as a large amount of process waste and equipment corrosion [8].

The importance of strong Brønsted acidic sites (SO_4^{2-}/–SO_3H) in the catalyst for cellulose acetylation has been suggested in the literature [9-11]. The Brønsted acid sites are hydroxyl groups with proton donor characteristics. As a result, proton transfer typically occurs at Brønsted locations [50]. According to the desired product, the acidity and textural properties of the heterogeneous catalysts can be adjusted [12]. Also, in comparison with the homogeneously catalyzed reactions, the strong Brønsted acidic sites provide high thermal, chemical, and mechanical stability [13]. In the past years, strong Brønsted solid acids such as sulfated zirconia, heteropoly acids, and Amberlyst-15 were applied successfully for cellulose acetate production [9-11]. Despite the successful utilization of heterogeneous catalysts, their efficiency was reported considerably lower than the homogeneous mineral acids [13]. This is because some heterogeneous catalysts are not selective and have low stability due to leaching. Other drawbacks such as solvent usage, product separation, large catalyst loading, and catalyst reusability were also realized [9-11]. As a green approach, development of active solid acid catalysts for cellulose acetate production gains importance.

The most common process for cellulose esterification is a solventless reaction because solvent will reduce the reaction rate by diluting modifiers. Moreover, solvent utilization complicates the product recovery and separation procedures after the reaction and leads to undesirable results by raising production costs. Furthermore, it is known that organic solvents are frequently hazardous to individuals and the environment. Consequently, the preference for a solvent-free reaction procedure is advantageous in many aspects [17, 18].

The objective of the present study is to develop a heterogeneous acid catalyst to produce acetone-soluble cellulose acetate, which has a degree of substitution between 2.2-2.7. For the solventless synthesis of cellulose acetate from microcrystalline cellulose, sulfated titania-silica (SO_4/TiO_2-SiO_2), sulfated La incorporated titania-silica (SO_4/La-TiO_2-SiO_2), sulfated Ti-SBA-15 catalysts (SO_4/Ti-SBA-15 and CSA/Ti-SBA-15) were

synthesized and tested. The effect of La incorporation on SO_4/TiO_2-SiO_2 catalyst and Si/Ti mole ratio on CSA/Ti-SBA-15 catalysts were investigated. The effect of Ti amount was also studied on the Ti-SBA-15 catalysts. Additionally, Ti-SBA-15 catalysts were prepared by different sulfate resources (ammonium sulfate and chlorosulfonic acid). For comparison purposes, commercial heterogeneous solid acid catalyst (Amberlyst-15) and homogeneous catalyst (H_2SO_4) were also tested on the cellulose acetylation reaction.

CHAPTER 2

CELLULOSE ACETATE

2.1. Cellulose and Cellulose Esters

2.1.1. Cellulose

Cellulose is the world's most abundant, renewable, and biodegradable organic polymer. In its native form, it serves as the structural material of the plant cell walls. Commercial cellulose is derived from highly pure sources such as cotton or wood, by the chemical pulping process. The cellulose content in cellulosic materials can be seen in Table 2.1 [1].

Table 2.1. The cellulose content in cellulosic materials [1].

Source	Cellulose content (%)
Cotton	90-99
Hemp	75-80
Bamboo	40-55
Bagasse	35-45

Cellulose, which is a linear polymer with the chemical formula of $(C_6H_{10}O_5)_n$, consists of long chains of repeating D-glucose units (also known as anhydroglucose units, AGU), that have bonded one another with the ß-1,4-glycosidic bonds. The cellulose chain length depends on the degree of polymerization (DP = n), which is the number of repeating glucose units [12]. As its molecular structure was illustrated in Figure 2.1, one chain end has an alcoholic hydroxyl (-OH) group on the C-4 carbon position, whereas the other end has a reducing hemiacetal group at the C-1 position. Cellulose includes three

reactive hydroxyl groups at the C-2, C-3, and C-6 atoms, which are accessible to the typical conversions of primary and secondary alcoholic -OH groups [8].

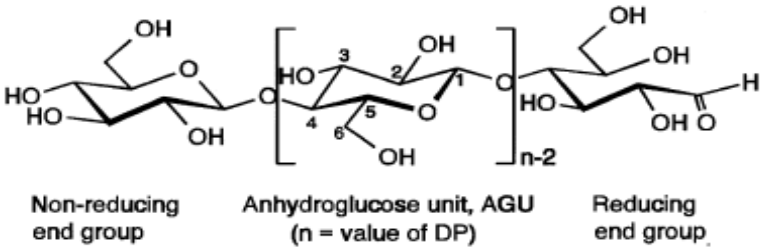

Figure 2.1. Molecular structure of cellulose [8].

The strong glycosidic bonds and the intra- and intermolecular hydrogen bonding provide cellulose not only its hydrophobic nature but also a high chemical and mechanical stability, making cellulose a suitable structural material [12]. Resulting from the presence of strong inter and intramolecular hydrogen bonds (Figure 2.2), native cellulose comprises highly crystalline regions and amorphous parts. The closely packed cellulose chains provide high crystallinity to the cellulose fiber, whereas the loosely packed molecules represent the amorphous region. Thus, although the hydroxyl groups in the amorphous regions are highly accessible and easily reactive in chemical reactions, the crystalline regions are not easily accessible by the reactants [1]. This highly crystalline structure both provides lower solvent solubility of cellulose and decreases the accessibility of reactive hydroxyl groups for chemical transformations [19, 13]. For cellulose to be used in the industry, cellulose must be converted to its derivatives [2, 3].

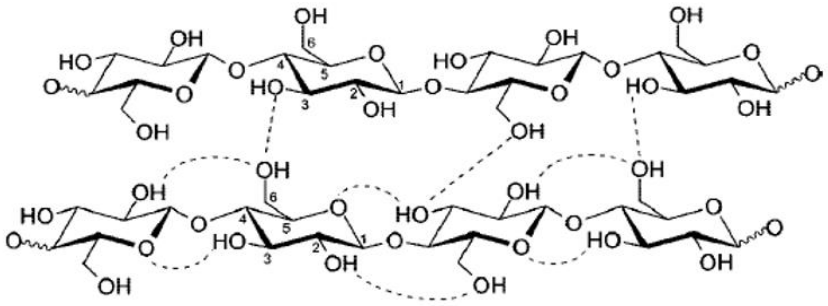

Figure 2.2. Intra- and intermolecular hydrogen bonds in cellulose [12].

Cellulose has a wide variety of functionalization pathways. In other words, the hydroxyl groups provide many reactions with reactive functional groups and thus form various valuable products. Through functionalization, cellulose can be converted into esters, ethers, silylates, sulfates, carbanilates, sulfonates, amines, azides, and hemiacetals, as given in Figure 2.3 [12]. Out of the cellulose derivatives, cellulose esters are commonly used in the industry in many areas such as coatings, membranes, composites, explosives, optical films, medical applications, food industry, or heavy metal sorption. The ester properties are affected by the type, distribution, and uniformity of the substituting group [1]. Cellulose ester derivatives are acetates, carboxymethylates, benzoylates, carbamates, (meth)acrylates, carbonates, sulfates, sulfonates, phthalates, tritylates, furorates, maleated esters, or ester resins [12].

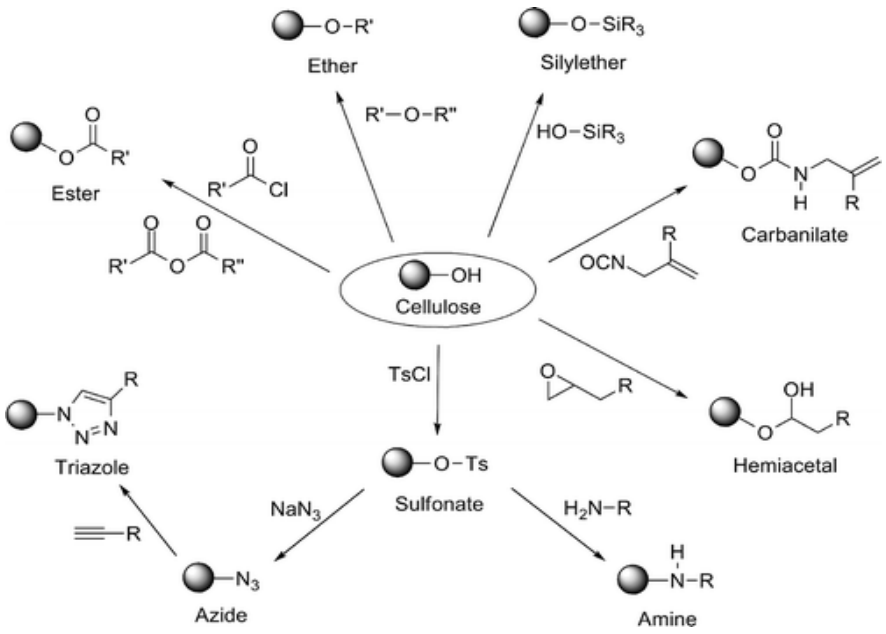

Figure 2.3. Functionalization routes of cellulose [12].

2.1.2. Cellulose Acetate

Cellulose acetate, also known as cellulose diacetate or as acetate, is a non-toxic and biodegradable chemical derived from cellulosic sources. Cellulose acetate (CA) has drawn great interest in the industry, not only because it's been an environmentally

friendly cellulosic resin but also being highly safe for living organisms [20]. Cellulose acetate is synthesized by the chemical modification of cellulose hydroxyl groups with the acetyl groups in the acetylating agent. The structural formula of cellulose acetate is illustrated in Figure 2.4. The number of substituted hydroxyl groups with the acetyl groups is the degree of substitution (DS), which can be a maximum of 3 since there are three hydroxyl groups in one cellulose AGU. The widely produced cellulose acetates in the industry are cellulose triacetate (CTA), and cellulose diacetate (CDA). CTA has an acetate group on almost every hydroxyl group, whereas CDA has partially substituted hydroxyl groups.

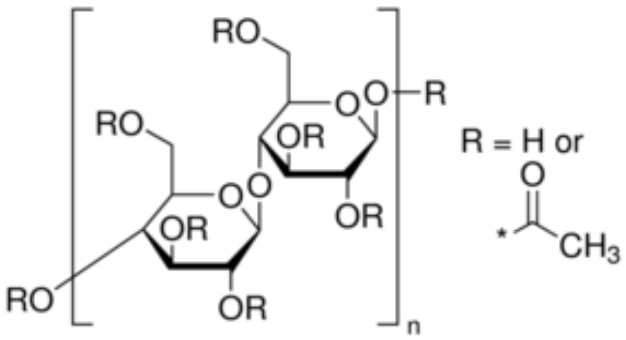

Figure 2.4. Chemical structure of cellulose acetate [21].

The DS affects the solvent solubility of cellulose acetate. The commonly utilized cellulose diacetate is soluble in acetone and has approximately 2.2–2.7 acetyl groups per every three hydroxyls. The effect of DS values on the solvent solubility of cellulose acetate is summarized in Table 2.2. As the DS of cellulose acetate decreases, CA becomes more water sensitive thus, their water dispersibility increases. On the other hand, derivatives having DS approaching 3.0, have lower water absorption and water solubility, but their solubility in organic solvents raises [1].

Table 2.2. Effect of degree of substitution on solvent solubility of cellulose acetate [8, 22].

Degree of Substitution (DS)	Common Solvent
2.8-3.0	Chloroform
2.2-2.7	Acetone

Table 2.3. (cont'd) Effect of degree of substitution on solvent solubility of cellulose acetate [8, 22].

Degree of Substitution (DS)	Common Solvent
1.2-1.8	2-Methoxy ethanol
0.6-1.0	Water

In the industry, cellulose is acetylated directly to the triacetate stage using an excess of acetic anhydride, acetic acid, and a homogeneous catalyst, then saponified to the diacetate. Because cellulose acetylation is a reversible reaction, the absence of water is essential for the reaction to complete [1].

Over the years, many solvent systems for homogeneous cellulose derivatization using acetic anhydride and sulfuric acid as the catalyst have been developed, including N, N-dimethylacetamide–lithium chloride (DMAc–LiCl) or dimethyl sulfoxide–tetrabutylammonium fluoride (DMSO–TBAF) [3]. Not only a significant amount of pollution is generated by the treatment of waste sulfuric acid after the reaction, but also these systems are not green solvents [9, 28].

The acetic acid process is the most extensively used method for industrial cellulose acetate production. In this method, cellulose is first swollen in acetic acid then acetylated using acetic anhydride in excess stoichiometric quantities and catalyzed by sulfuric acid or perchloric acid catalysts [18]. Under acidic circumstances, the acetal group in the cellulose backbone tends to hydrolyze therefore, some polymeric chain breakdown is unavoidable. Because of the nature of the mineral acid-catalyzed reactions, it is also difficult to directly synthesize the partially substituted cellulose acetates therefore, the commercially desired acetone-soluble cellulose diacetates (CDA) are synthesized by hydrolyzing completely substituted CTA by a multistep process [13]. Following partial hydrolysis of the cellulose triacetate, cellulose diacetates with lower DS (2.0–2.5) are produced. Large amounts of waste was created because of the two-step commercial method and certain material qualities may have been lost owing to molecular weight degradation [28]. Furthermore, employing lower amounts of the acetylating agent to produce directly produced cellulose diacetate led to an inhomogeneous functional group distribution throughout the chain, resulting in irreproducible product characteristics, making it unsuitable for commercial processing [28].

Although the acetic acid process has low cost and high productivity, serious cellulose degradation and hydrolysis of cellulose acetate are inescapable due to the water and remaining acid catalysts in the hydrolysis step. Therefore, despite the widespread availability of CA and established commercial manufacturing process, its synthesis techniques require additional investigation [11, 18].

2.1.2.1. History of Cellulose Acetate

The acetylation of cellulose by acetic anhydride was found by Paul Schützenberger and Laurent Naudin in 1865. In 1894, Cross and Bevan patented a procedure for making chloroform-soluble cellulose triacetate. In the form of safety film, cellulose diacetate was first used commercially as plastic in motion-picture photography in the 1920s. During World War I, Henri and Camille Dreyfus established a cellulose diacetate plant in England, to be used as a nonflammable “dope” for coating fabric airplane wings. After the war in 1921, diacetate fiber production started with the name Celanese. In 1929, acetate fiber was produced in the United States by DuPont and won widespread popularity because of its softness and resistance to wrinkle and staining [23].

2.1.2.2. Usage Areas of Cellulose Acetate

Depending on how it's processed, cellulose acetate may be utilized in a variety of ways. Cellulose diacetate is used to produce fibers and membranes. The filtration membranes are produced from cellulose triacetate molded into a film or hollow thread form. Cellulose acetate became often used in the automotive industry through its mechanical strength, toughness, wear resistance, transparency, and ease of moldability. Due to it has low plasticity, it is mixed with plasticizers before extruded or injection-molding processes. Thus, it has traditionally been utilized in products such as eyeglass frames and combs [23]. The usage areas of cellulose acetate can be seen in Table 2.3.

Table 2.4. Usage areas of cellulose acetate [23].

Usage Area	Product	Used for
Textiles	Acetate fabrics	Soft texture, high absorptive capacity
Plastic applications	Film or sheet	Packaging, photographic film, eyeglass frames
Tobacco industry	Diacetate tow	Filtration properties, taste acceptance
Cosmetics	Microbeads	Smooth texture, good dispersibility
Membrane technology	Membranes	Seawater desalination, drinking water purification, wastewater treatment
Pharmaceuticals	Semipermeable membrane	Controlled-release tablets

2.1.2.3. Physical Properties of Cellulose Acetate

Cellulose acetate is flame resistant and has a high melting point, allowing it to melt and carbonize at temperatures ranging from 230 °C to 300 °C. Because of its low electrical conductivity and high internal and exterior resistance, it is an excellent insulating material. Also, it has resistance to chemicals and solvents. Cellulose acetate-based products such as fabrics, molded items, coated film, and paints are very resistant to sunlight (UV radiation), do not degrade readily, and may thus be used for extended periods. Due to its properties such as high mechanical strength and high dielectric constant (transparency), it is suitable for manufacturing a wide range of products [20]. The physical properties of cellulose acetate are given in Table 2.4.

Table 2.5. General physical properties of cellulose acetate [24].

Item	Property
Shape	White and flaky
Bulk density (kg/l)	0.25-0.52
Melting point (°C)	230-300
Glass transition temperature (°C)	160-180
Specific heat (kJ/kg·K)	1.34

2.1.2.4. Cellulose Acetate Market

Cellulose acetate (CA) acts as a major market trend in various industries. The worldwide cellulose acetate market was worth $6.15 billion in 2020 and is predicted to be $10.25 billion by 2028, growing 8.9 % between 2021 and 2028. The forecast for 2022 market is more than $7 billion [25]. The market is being driven by the demand from the textile and cigarette industries. With the rising usage of cellulose acetate in tapes and labels, Asia-Pacific is expected to be the leader cellulose acetate market over the next decade. Europe is anticipated to be the second-largest cellulose acetate market because of the consistent rate of production and the availability of distribution channels. Due to environmental concerns, biodegradable plastic is being requested, which will also be increasing the use of cellulose acetate plastic worldwide. The food packaging and eyeglass frame industries are also expected to drive market expansion in the future [25, 26].

2.2. Reaction Mechanism of Cellulose Acetylation

Cellulose acetate synthesis mechanism is illustrated in Figure 2.5. Firstly, the Brønsted acidic catalyst activates the acetic anhydride carbonyl group by giving its proton (H^+) to it. The hydroxyl groups in cellulose were then replaced with acetate groups of acetic anhydride. The production of an intermediate between cellulose, acetic anhydride, and the acidic catalyst is proposed as the reaction mechanism. The triple arrow indicates numerous stages in the reaction [9, 27].

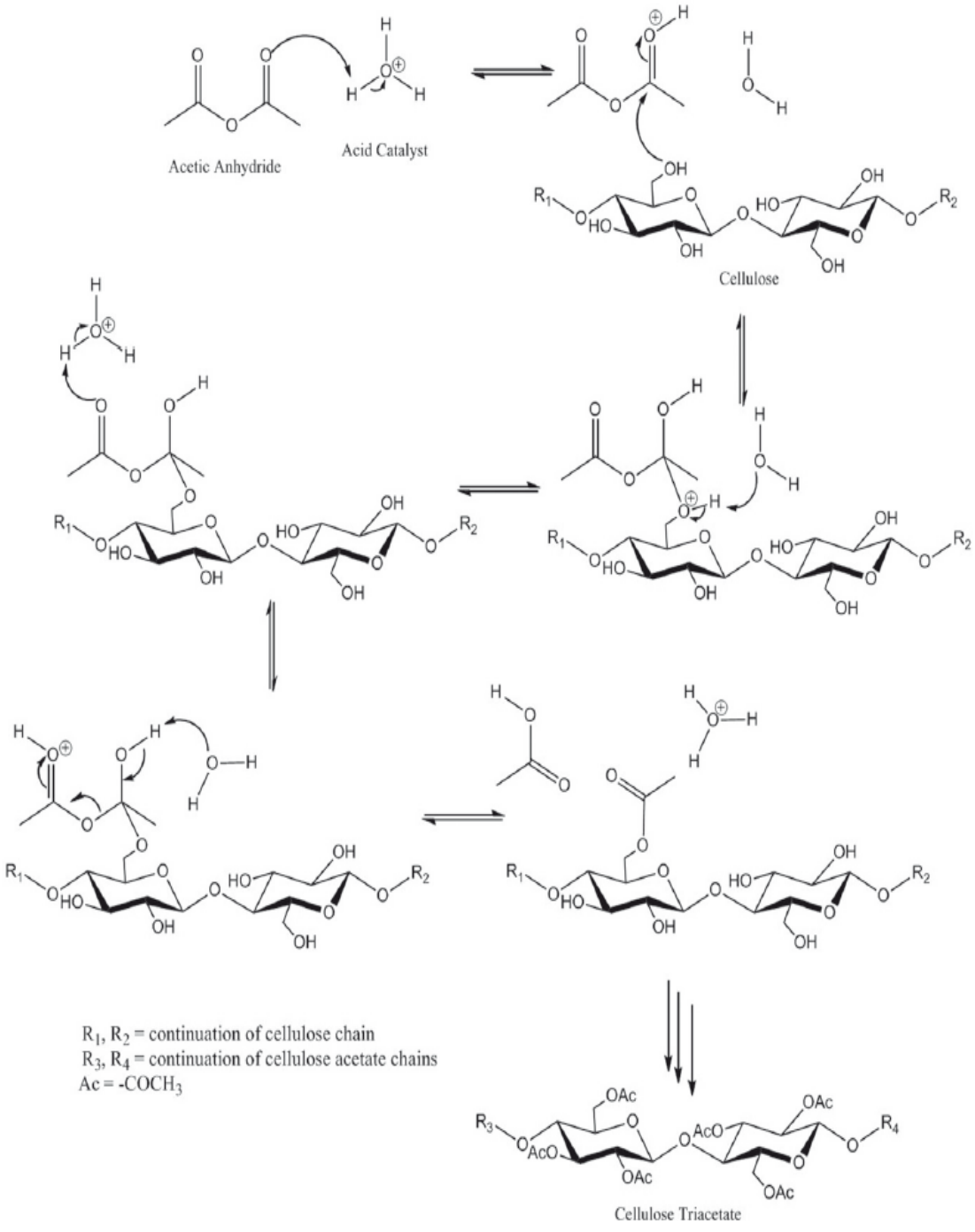

Figure 2.5. The schematic diagram of the cellulose acetate synthesis mechanism [22].

CHAPTER 3

LITERATURE SURVEY ON PRODUCTION OF CELLULOSE ACETATE

3.1. Studies on Homogeneous Catalysts

In general, homogeneous cellulose modifications allow for greater control of the DS and cellulose regioselectivity in terms of primary vs. secondary hydroxyls, as well as homogenous functionalization throughout the polymer chain [28]. The synthesis of partially substituted cellulose acetate with mineral acid catalysts is unfeasible due to the nature of the mineral acid-catalyzed reaction [7]. Hence, the commercial acetone-soluble cellulose diacetates (CDA) are produced by the hydrolysis of completely substituted cellulose triacetate (CTA), via a multi-step method [7].

In Chapter 2, it was reported that cellulose acetate production is carried out with sulfuric acid catalyst, acetic acid, an excess of acetic anhydride, and perhaps with solvents such as dimethyl sulfoxide–tetrabutylammonium fluoride (DMSO–TBAF), or LiCl/N, N-dimethylacetamide (LiCl/DMAc). However, because sulfuric acid is not recoverable after the reaction and the solvent systems are not environmentally friendly, a significant quantity of pollution is generated [28].

Several ionic liquids (ILs) are considered “greener” solvents for cellulose dissolution and functionalization. They are “green” solvents due to their low vapor pressure, non-flammability, and high thermal stability. Ionic liquids (IL’s) are organic salts consisting of anionic (chloride, acetate, formate, and alkyl phosphate) and cationic (imidazolium, pyridinium, and pyrrolidinium) groups. IL’s weaken the inter-and intramolecular hydrogen bonds of cellulose, causing its dissolution. The cellulose dissolution mechanism proceeds through hydrogen bond formation between the anion of IL and cellulose hydroxyl groups. IL’s are known as non-derivatizing solvents because the dissolution mechanism occurs by intermolecular interaction [29].

Heinze et al. (2005) utilized acidic ionic liquid 1-butyl-3-methylimidazolium chloride ($[BMIM^+]Cl^-$) as the reaction medium for homogeneous cellulose acetate production [30]. The experiment was carried out at 80°C for 2 h and acetic anhydride was used to esterify microcrystalline cellulose. Although a product yield of 85.9 % and a DS of 2.72 were obtained, the synthesis of acidic ionic liquids (IL's) was reported to be an expensive process. Moreover, the study also indicated that the ease of contamination of ILs throughout the process not only complicates the IL recovery, but also product separation [28].

Biswas et al. (2006) investigated the conversion of cellulose into cellulose triacetate from rice straw, wheat hull, and corn fiber cellulose [31]. In an acetic acid and methylene chloride medium, the reaction was carried out for 4 h at 80 °C with excess acetic anhydride and 0.04 g sulfuric acid (H_2SO_4). Cellulose triacetate was easily recovered from the unreacted substrate since it is soluble in methylene chloride or chloroform. The degree of substitution of cellulose acetate from all three sources was determined to be 2.8, as confirmed by proton NMR. The H_2SO_4 treatment makes the cellulose more accessible to acetic anhydride, making it more reactive to acylation.

Fan et al. (2013) studied the impact of phosphotungstic acid ($H_3PW_{12}O_{40}\cdot 6H_2O$) on cellulose acetylation in dichloromethane with acetic anhydride [10]. The reaction was carried out at 45 ^oC under reflux for 6 h. Rice straw cellulose was acetylated using a process similar to described in the study of Biswas et al. (2006) [31]. Table 3.1 reveals that the strong acidity (lower pKa) of inorganic strong acids were responsible for full cellulose acetylation. In the presence of sulfuric acid (H_2SO_4) and perchloric acid ($HClO_4$) catalyzed reaction, cellulose acetates with DS of 2.92 and 2.83 were synthesized, respectively. Due to its insolubility and poor acidity, tungstic acid (H_2WO_4 or $WO_3\cdot H_2O$) yielded almost no activity. On the other hand, phosphotungstic acid was shown to be an active catalyst for the acetylation of treated rice straw, because of its comparatively significant Brønsted acidity. Under the same reaction conditions, a DS of 2.25, and a yield of 27.8 % were obtained. The presence of inorganic strong acid as the catalyst resulted in complete cellulose OH group substitution, however, phosphotungstic acid contributed to partial substitution.

Considering the dependence of the acetylation of the treated rice straw on the phosphotungstic acid amount, results in Table 3.1 indicated that the yield of cellulose acetate increased with an increasing catalyst loading. However, the DS values were nearly

consistent in the beginning (acid/AGU molar ratios of 0.10 and 0.15). A decrease in DS was observed when the acid/AGU molar ratio exceeded 0.15.

When the acid/AGU molar ratio was 0.3, there was a substantial decline in DS of 1.43. The maximum CA production, on the other hand, was 41.1 % at an acid/AGU molar ratio of 0.3. It is well known that increasing the acid concentration improves cellulose acetylation, hence an increase in yield was observed. Because the hydrated compound $H_3PW_{12}O_{40}\cdot 6H_2O$ was utilized as the catalyst, the results of DS and yield were inversely proportional above an acid/AGU molar ratio of 0.15. This was attributed to the elevated acid concentration and water quantity in the reaction system. The presence of water especially in the acidic and high-temperature reaction conditions causes cellulose chain degradation, therefore, resulting in a low DS [32].

Table 3.1. Acetylation of treated rice straw catalyzed by various catalysts [a] [10].

Catalyst	Acid/AGU (molar ratio)	Yield (%)[b]	DS
H_2SO_4	0.2	29.1	2.92
$HClO_4$	0.2	31.5	2.83
H_2WO_4	0.2	–	–
$H_3PW_{12}O_{40}\cdot 6H_2O$	0.2	27.8	2.25
$H_3PW_{12}O_{40}\cdot 6H_2O$	0.1	15.8	2.08
$H_3PW_{12}O_{40}\cdot 6H_2O$	0.15	20.6	2.22
$H_3PW_{12}O_{40}\cdot 6H_2O$	0.25	34.3	1.92
$H_3PW_{12}O_{40}\cdot 6H_2O$	0.3	41.1	1.43

[a] Reaction conditions: 2 g of cellulose (about 12.3 mmol AGU), 0.5 g of acetic acid, 5 g of acetic anhydride, reflux in 30 ml CH_2Cl_2 for 6 h.

[b] The yield of cellulose acetate was calculated based on the complete cellulose substitution.

Although strong Brønsted acidity of phosphotungstic had a positive impact on cellulose acetylation, a large catalyst amount was required; also, the catalyst-to-cellulose molar ratio reached 20 %. Moreover, due to the homogeneous nature of phosphotungstic acid, the catalyst was not recoverable after the acetylation process.

3.2. Studies on Heterogeneous Catalysts

Konwar et al. (2016) studied the effect of sulfonated carbon catalysts (-SO_3H) on the solventless esterification of microcrystalline cellulose with acetic anhydride [13]. The reactions were carried out at 80 ^oC, under mechanical stirring (1000 rpm) for 12 h in solvent-free conditions with acetic anhydride (Ac_2O): AGU mole ratios of 9:1 and 4.5:1. Mesoporous active carbon, derived with hydrothermal method from Pongamia glabra cake, and commercial mesoporous active carbon were sulfonated using 4-benzene diazonium sulfonate (4-BDS) for the synthesis of the -SO_3H acid-functionalized mesoporous carbons and were named as AC500S and CACS, respectively. The comparison of prepared catalysts, commercial zeolites, and active carbon was given in Table 3.2.

According to Table 3.2, zeolites have shown low cellulose acetylation activity, which was related to the penetration of large polymeric cellulose molecules to the catalyst's strong (active) acid sites located in tiny micropores would be nearly impossible. Compared to active carbon (AC500), its sulfated form AC500S gave a CA yield of 77 %, due to its large pore size (4.8 nm) and primarily its sulfonic acid density (0.82 mmol/gcatalyst). Also, it was observed that the Brønsted acid site strength is directly proportional to the activation of the acetic anhydride molecules, and thus the CA yield. Comparing the acidity of AC500S and CACS catalysts, AC500S had 6.07 mmol/gcatalyst and CACS has 5.12 mmol/gcatalyst acidity. Thus, AC500S had given a 27 % higher cellulose acetate yield than CACS. Although AC500S and CACS had smaller pore sizes than cellulose critical diameter (~10 nm), they contain pores greater than 10 nm and gave high activity in acetylation.

Table 3.2. Catalyst properties and yield of obtained cellulose acetate [13].

Catalyst	Acidity (mmol/ gcatalyst)	-SO_3H (mmol/ g)	Surface Area (m^2/g)	Pore diameter (nm)	Yield (%)	DS
H-ZSM-5 Zeolite	1.14	-	443	0.6	0	-
H-Y Zeolite	0.83	-	884	0.8	0	-
Commercial Active Carbon (CAC)	1.10	-	201	5.5	0	-

Table 3.2. (cont'd) Catalyst properties and yield of obtained cellulose acetate [13].

Catalyst	Acidity (mmol/ gcatalyst)	-SO_3H (mmol/ g)	Surface Area (m^2/g)	Pore diameter (nm)	Yield (%)	DS
Sulfonated Commercial Active Carbon (CACS)	5.12	0.53	119	4.0	50	2.10
Active Carbon (AC500)	1.17	-	820	4.7	0	-
Sulfonated Active Carbon (AC500S)	6.07	0.82	483	4.8	77	2.94

The effect of reaction time and Ac_2O: AGU mole ratio on the DS and catalyst loading on the DS and yield were given in Figure 3.1 (a) and (b). The amount of acetic anhydride was found to be directly proportional to DS because the equilibrium shifts to the product side. Similarly, an increase in catalyst loading resulted in a higher yield and DS of CA. The change in the reaction temperature (80 ^oC and 100 ^oC) did not affect product yield and DS. Incomplete or partial cellulose conversion was observed when the Ac_2O/AGU molar ratio was less than 4.5. The reactivity of the AGU hydroxyl groups was determined by comparing the various $–CH_3$ signals (C2, C3, and C6) of AGU. The DS of the different –OH groups revealed that the order of reactivity was C6–OH > C2–OH > C3–OH. A cellulose acetate yield of 77 % and DS of 2.94 were obtained by using an AC500S catalyst with the following optimized reaction conditions: a duration of 12 h, Ac_2O: AGU mole ratio of 9:1, and catalyst to cellulose ratio (w/w) of 1. During three reaction cycles, sulfonated materials demonstrate good stability, with consistent DS and CA yields.

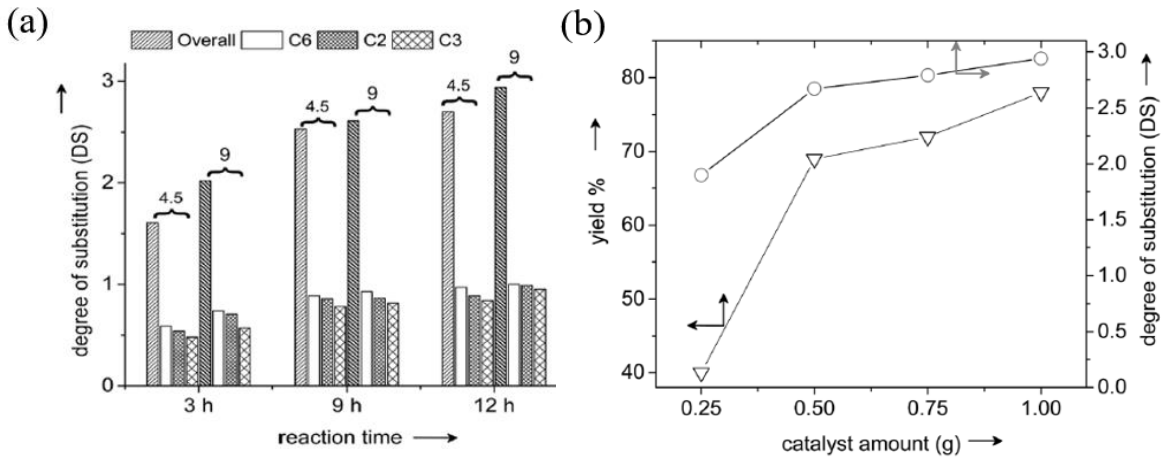

Figure 3.1. (a) Effect of time and Ac_2O: AGU mole ratio on DS (80 ^oC) (b) Effect of catalyst loading on DS and yield (12 h, 80 ^oC, Ac_2O/AGU=9:1) [13].

The FT-IR and TGA patterns of CA were illustrated in Figure 3.2. The TGA pattern in Figure 3.2. (a) indicates one major weight loss in the range of 300-400 ºC due to polymer decomposition. The decomposition temperature and thus the thermal stability of CA was observed to be higher than the pure microcrystalline cellulose. This finding implies that the substitution of hydroxyl groups with acetyl groups has affected the thermal stabilities of cellulosic materials [11]. Cellulose acetate formation was confirmed by the FT-IR analysis where the C=O acetate peak at 1750 cm^{-1} and a decreased –OH stretch signal near 3400 cm^{-1} of CA was given in Figure 3.2 (b).

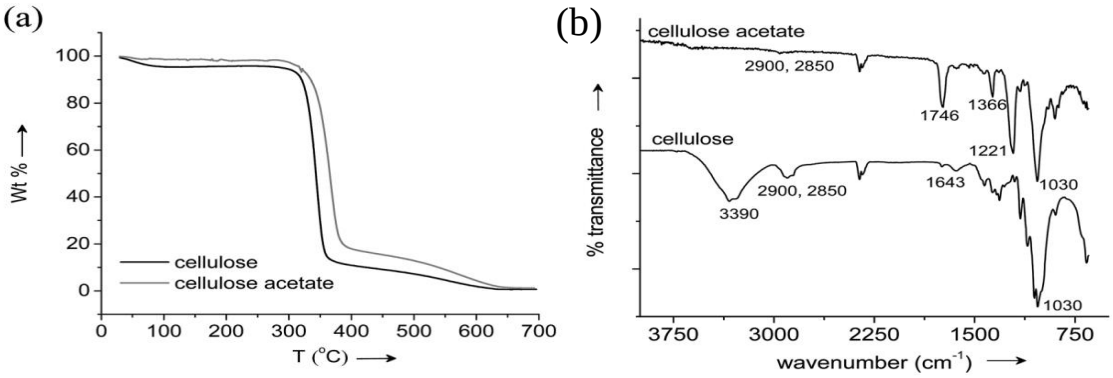

Figure 3.2. (a) TGA pattern of CA sample obtained with sulfonated carbon catalyst (AC500S). (b) FT-IR spectra of CA sample obtained with sulfonated carbon catalyst (AC500S) [13].

Meng et al. (2017) investigated the effect of calcination conditions on the structure and activity of SO_4^{2-}/TiO_2 solid acid catalyst for cellulose acetylation reaction. SO_4^{2-}/TiO_2 catalyst was synthesized by the sol-gel method [33]. Titanium sulfate [$Ti(SO_4)_2$] was employed as the starting material in this study, hence eliminating the step of H_2SO_4 treatment. The reaction was carried out by using acetic anhydride, acetic acid, and a supercritical activator (1,1, 1,2- tetrafluoro ethane). The effect of calcination temperature of the SO_4^{2-}/TiO_2 catalysts is shown by the XRD analysis given in Figure 3.3.

The catalyst shows an amorphous structure below the calcination temperature of 350 ºC, which was catalytically inert. As the calcination temperature was increased, the transformation from amorphous TiO_2 to anatase TiO_2 was observed. Anatase TiO_2 is well recognized for its high crystallinity and high catalytic activity. The peak at $2\theta = 25.4°$ was the most stable (101) plane of anatase. After 500 °C, the characteristic anatase diffraction peaks were completely observable in the XRD patterns. It was also

demonstrated that catalyst deactivation occurred above 550 °C due to SO_4^{2-} decomposition on the catalyst surface. Allowing the amorphous structure to change into an anatase crystal, enhanced catalytic performance with higher crystallinity was observed when the SO_4^{2-}/TiO_2 catalyst was calcined at 500 °C for 6 h.

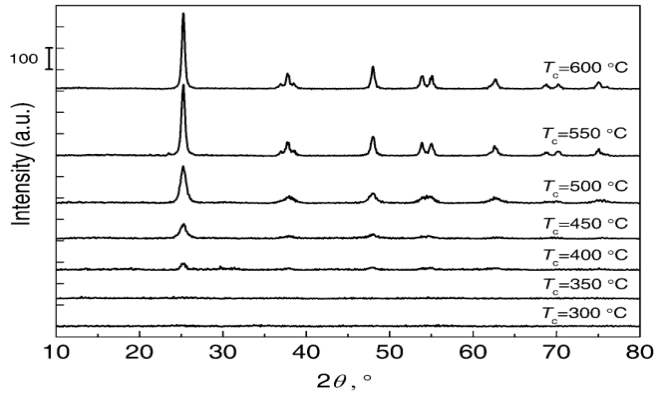

Figure 3.3. XRD patterns of SO_4^{2-}/TiO_2 catalysts calcined at different temperatures [33].

To investigate the acidic strength of the SO_4^{2-}/TiO_2 solid acid catalyst, NH_3-TPD analysis was conducted for fresh, and 4 times reused catalyst. The NH_3-TPD results are given in Figure 3.4. After four reaction runs, the acidity of the SO_4^{2-}/TiO_2 catalyst dropped by 6 % compared to the fresh catalyst. Furthermore, it can be noted that the minor change between the two profiles occurred below 400 ^oC due to weak and moderate acid sites. The acidity of the strong acid site at 400 ^oC dropped by 1.3 %, which did not affect SO_4^{2-}/TiO_2 activity. The findings revealed that some SO_4^{2-} leached during the acetylation process utilizing an SO_4^{2-}/TiO_2 solid acid catalyst. The conversion of cellulose has been accomplished at 110 ^oC and 5 MPa pressure, in 1.5 h with a cellulose acetate yield of 100 % and DS of 2.94.

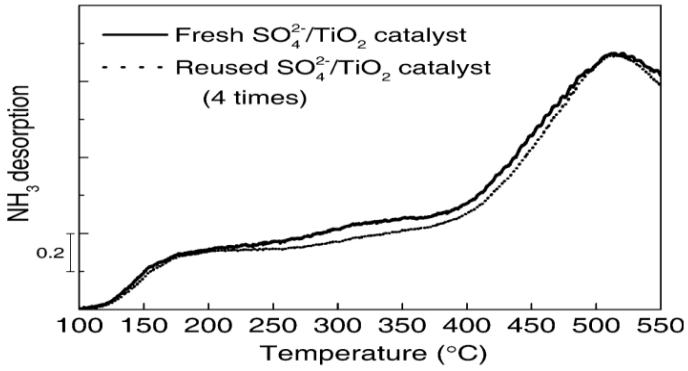

Figure 3.4. NH_3-TPD graph of fresh and four times reused SO_4^{2-}/TiO_2 catalyst [33].

In the study of Yan et al. (2006), solvent-free cellulose acetate production with acetic anhydride and solid superacid SO_4^{2-}/ZrO_2 was investigated [9]. The sulfation of ZrO_2 was carried out by H_2SO_4 and SO_4^{2-}/ZrO_2 was calcined in air at 550 ^oC for 3 h. The reaction was carried out at room temperature for 7.5 h. The cellulose to Ac_2O ratio (w/w) was 1.62 and the cellulose to catalyst ratio (w/w) was 5.53. The reaction was carried out in a ball-mill reactor, for the activation of cellulose -OH groups by increasing the cellulose surface area. The FT-IR spectra results confirmed that the ball-milling technique has reduced the crystallinity and degree of polymerization (DP) of the cellulose, as given in Figure 3.5. The intensity of the C=O acetate peak at 1750 cm^{-1} increased proportionally as the reaction duration was increased. This indicates that cellulose acetate DS is directly proportional to the prolonged reaction time. The synthesized cellulose acetate sample had a DS of 1.8 and a yield of 75.6 % in the acetylation reaction carried out for 7.5 h at room temperature.

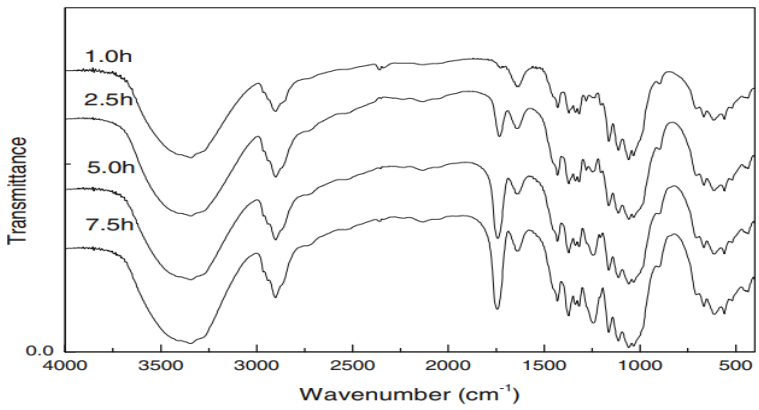

Figure 3.5. FT-IR spectra of cellulose acetate prepared by SO_4^{2-}/ZrO_2 at different reaction times [9].

Fan et al. (2014) used sulfonated Amberlyst-15 catalysts containing the sulfonic acid group to optimize the acetylation of cellulose extracted from rice straw [11]. Most resins are Brønsted acid catalysts with high ion exchange capacity, particularly Amberlyst-15. Dichloromethane was used as the solvent, and the reaction was carried out at 45 ^oC for 10 h. Both the FT-IR and TGA results of the fresh and recovered Amberlyst-15 catalyst indicated a highly stable chemical composition and structure during the acetylation process. According to Figure 3.6 (a), up to 200°C, a weight loss in the sample was observed due to the removal of adsorbed water. The second mass loss up to 400 °C was due to sulfonic acid group decomposition and polystyrene chain depolymerization.

The final weight loss was because of the polymer backbone breakdown. The mass loss of the recycled catalyst was found to be slightly less than the fresh catalyst, indicating its stability. FT-IR spectra of the fresh and recovered Amberlyst-15 catalyst given in Figure 3.6 (b) illustrates the presence of characteristic peaks due to stretching vibrations of -OH groups (3426 cm^{-1}); C-H in $-CH_2-$ units (2926 cm^{-1}); SO_3 groups (1128-1038 cm^{-1}); and aromatic moieties (1413–1641 and 672–906 cm^{-1}).

Amberlyst-15 catalyst underwent a minor chemical change during the acetylation process. SEM (Scanning Electron Microscopy) analysis of the fresh and recovered catalysts indicated that, at low magnification, the fresh catalyst had a smooth surface morphology, however, several cracks were visible on the surface of the recovered catalyst. Because of the poor mechanical strength of the commercial Amberlyst-15 catalysts, they may not be strong enough to withstand the violent stirring throughout the reaction. At greater magnifications, only particle aggregation was detected, showing that the reaction had no effect on the catalyst microstructure. According to the TG-DTG analysis, a minor quantity of unreacted cellulose was also found on the surface of the recovered catalyst [11].

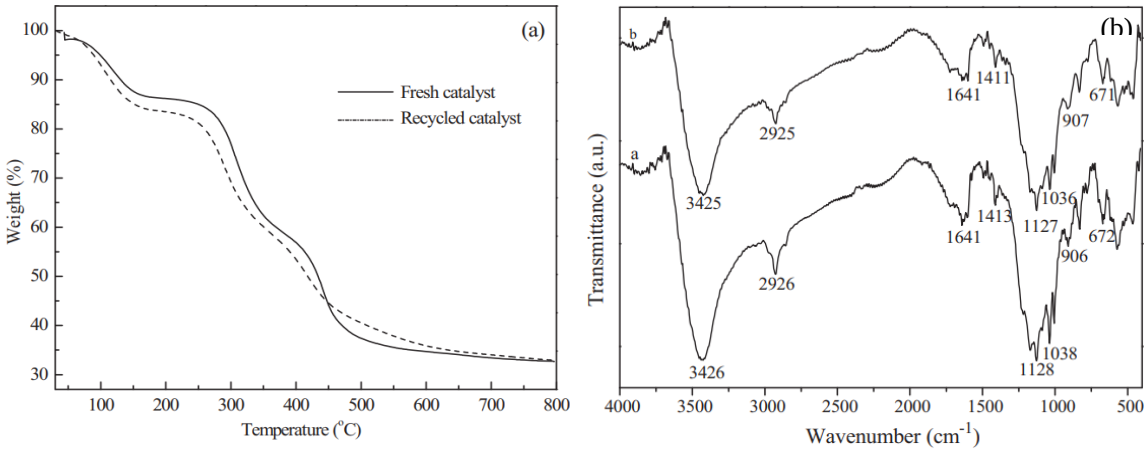

Figure 3.6. (a) TGA curve of the fresh and recovered catalyst after the fourth run. (b) FT-IR spectra of Amberlyst 15 catalyst fresh [a] and recovered [b] catalyst after the fourth run [11].

Table 3.3 illustrates the effect of catalyst amount on DS and yield. The increase in the catalyst amount at the reaction conditions of 45 °C and 10 h resulted in both improved DS value and yield. Using 1.5 g of Amberlyst-15, a DS value of 2.27 and a

yield of 43.9 % were observed. However, a further increase in the catalyst loading resulted in a decrease in both DS and yield. It was concluded that the larger catalyst amount led to cellulose acetate degradation, which occurs due to the ß-1,4-glycosidic bond scission, and then the anhydroglucose unit breakage and acetic acid evolution due to partial deacetylation [34]. Moreover, during the reaction, a small amount of formed unstable cellulose resulted in the breakdown of macromolecular cellulose into smaller molecular glycolipids [35]. As a result, the DS value and yield of cellulose acetate decreased.

Table 3.3. Cellulose acetylation with various Amberlyst-15 catalyst loading [11] (2 g of cellulose, AGU: acetic acid: acetic anhydride = 1:0.8:4 (molar ratio), reflux in 50 ml CH_2Cl_2 at 45 ^oC for 10 h).

Catalyst Amount (g)	DS	Yield (%)
0.5	0.68	11.2
1.0	1.78	36.4
1.5	2.27	43.9
2.0	1.44	38.2
2.5	0.93	14.5

Table 3.4 illustrates the effect of reaction time and acetic anhydride to AGU unit molar ratio on the cellulose acetate DS and yield. As the reaction time increased from 4 to 10 h, an enhancement in the cellulose acetate yield by 27.7 % and DS by 0.45 were observed accordingly. The highest CA yield and DS were obtained at 10 h reaction time as 43.9 % and 2.27, respectively. When the reaction time was increased above 10 h, a decline in the product yield was observed, which was attributed to the increased possibility of cellulose breakdown [10]. Table 3.4 also shows how the amount of acetic anhydride affected cellulose acetylation. With the increasing acetic anhydride to AGU unit molar ratio from 3:1 to 7:1, both the CA yield and DS were found to be increasing from 39.5 % to 54.1 % and from 1.83 to 2.38, respectively. The higher amounts of acetic anhydride used facilitate the reaction equilibrium to shift to the right (product) side, resulting in more cellulose acetylation thus yield and DS enhancement of the cellulose acetate.

Table 3.4. Effect of reaction conditions on cellulose acetylation [11]. (2 g of cellulose, 1.5 g of Amberlyst-15)

Reaction Time (h)	$\frac{n_{\text{Acetic Anhydride}}}{n_{\text{AGU}}}$ (molar ratio)	DS	Yield (%)
4	4	1.82	16.2
6		2.03	26.9
8		2.24	35.9
10		2.27	43.9
11		2.25	32.8
12		2.28	25.3
10	3	1.83	39.5
	5	2.38	48.6
	6	2.35	52.8
	7	2.38	54.1

Throughout four reaction cycles carried out at 45 ^{o}C for 10 h, no significant differences in the DS values were observed and consistent yields of cellulose acetate were obtained. Under optimized reaction conditions, CA with DS of 2.38 and a yield of 54.1 % was produced.

3.2.1. Sulfated Ti-SBA-15 Catalysts

Considering its hexagonal shape and mesoporous pore structure, SBA-15 silica material was chosen for this work as the catalyst support. An organic copolymer was used to arrange the structure of a polymeric silica precursor template, which was used to create this material. Because it has a more uniform structure and thicker walls, SBA-15 has significantly greater stability than MCM-41 [14]. Despite the low catalytic activity of pure siliceous SBA-15 materials possess, the introduction of metal (Fe, Ti, Zn, Cu) or other active ingredients such as heteropoly acid, provided acidity and improved the catalyst stability and catalytic activity [16]. Many researchers have recently incorporated

metals or other acid functional groups into pore structures to modify the characteristics of mesoporous molecular sieves. It was reported by Mutlu et al. that Zr–SBA-15 used as a catalyst for the esterification of cetyl alcohol with palmitic acid resulted in a 63.1 % yield [39].

The pore size and volume of mesoporous SBA-15 are not only affected by the synthesis temperature, but also employment of various of poly (alkylene oxide) triblock copolymers. To acquire a two-dimensional hexagonal structure, the catalyst was synthesized in an acidic medium [14]. Figure 3.7 illustrates the preparation steps of SBA-15.

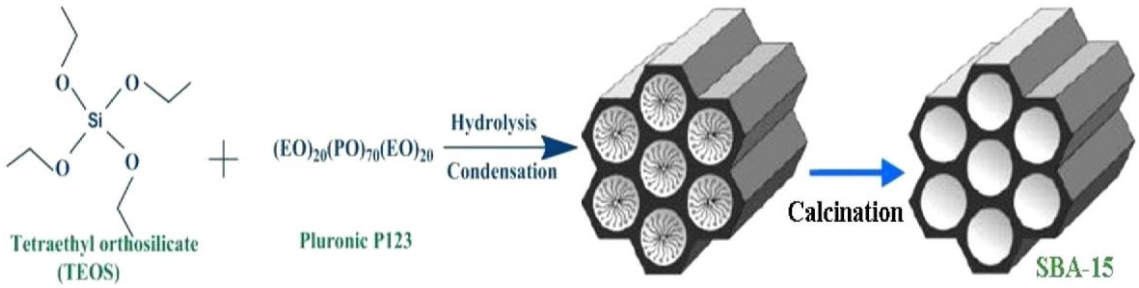

Figure 3.7. SBA-15 preparation steps [40].

Zhao et al. (1998) investigated the synthesis of well-ordered hexagonal mesoporous silica (SBA-15) that has pores between 5 to 30 nm. Amphiphilic (both hydrophilic and hydrophobic) surfactant pluronic (P123), which is a poly(ethylene oxide) (PEO) and poly(propylene oxide) (PPO) block copolymer (PEO–PPO–PEO), was used to synthesize SBA-15. When the synthesis temperature was under 25 °C amorphous silica was obtained, whereas above 80 °C silica gel formation was observed. It was stated that due to protonation or temperature-dependent hydrophilicity of the PEO block of the copolymer under the acidic synthesis conditions, or a combination of both higher temperatures or longer reaction times results in larger pore sizes and thinner silica walls. After SBA-15 synthesis and air calcination at 500 °C, the mean pore size was 8.9 nm, pore volume was 1.17 cm^3/g, BET surface area was 850 m^2/g and pore wall thickness was 3.1 nm. Also, after calcination, it was observed that SBA-15 exhibited a well-ordered similar hexagonal array shape.

In another study, Sharma et al. (2013) synthesized Ti incorporated mesoporous SBA-15 (Ti-SBA-15) by the hydrothermal preparation technique for the ring-opening

reaction of epoxidized canola oil with acetic anhydride at 130 °C [41]. Catalyst stability and conversion were investigated for the Si/Ti molar ratios of Ti-SBA-15 (10, 20, 40, and 80). The textural characterization results of Ti-SBA-15 and sulfated Ti-SBA-15 catalyst are given in Table 3.5. By sulfation with chlorosulfonic acid, the specific surface area of Ti-SBA-15(10) was reduced from 993 to 594 m^2/g. Probably, this is related to the production of sulfate linkage in sulfated Ti-SBA-15(10) catalyst, which is also indicated by FT-IR spectra at 1388 cm^{-1} due to sulfate group vibration. The sulfated Ti-SBA-15(10) catalyst's specific surface area, mean pore volume, and pore diameter were reported to be 594 m^2/g, 0.99 cm^3/g, and 6.6 nm, respectively.

Table 3.5. Textural characterization of Ti-SBA-15 and SO_4/Ti-SBA-15 with different Si/Ti ratios (10–80) [41].

Catalyst[a]	S_{BET} (m^2/g)	d_P (nm)	V_P (cm^3/g)
Amorphous SiO_2	1011	2.3	0.59
SBA-15	864	6.4	1.03
Ti-SBA-15 (10)	993	5.5	1.36
Ti-SBA-15 (20)	989	5.4	1.36
Ti-SBA-15 (40)	1030	5.3	1.38
Ti-SBA-15 (80)	1066	5.5	1.49
Sulfated Ti-SBA-15 (10)	594	6.6	0.99

Considering its greater sulfate concentration and acidic strength, chlorosulfonic acid was used as the sulfating agent [42]. *S*ulfation of Ti-SBA-15 (10) was accomplished by treatment with 0.5 M solution of chlorosulfonic acid. After that, the catalyst was calcined at 550 °C. The acid sites of SO_4/Ti-SBA-15 and Ti-SBA-15(10) were confirmed with NH_3-TPD analysis which was illustrated in Figure 3.8. In the strong acid site, sulfated Ti-SBA-15(10) has a single wide peak at 220–390°C. This high temperature ammonia desorption was attributed to the existence of strong acidic sites in the catalyst, which was caused by the presence of sulfate linkage.

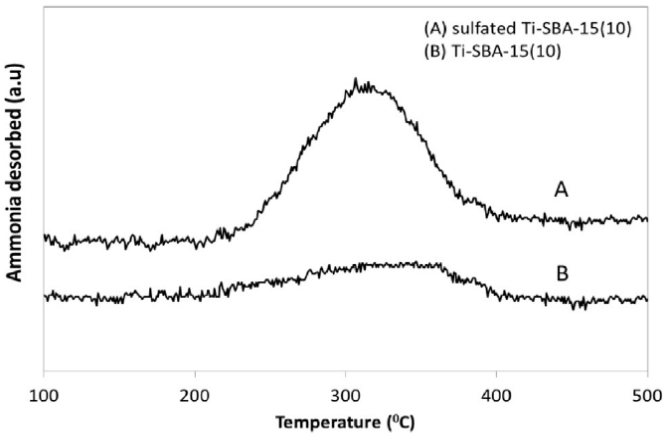

Figure 3.8. NH_3-TPD profile of SO_4/Ti-SBA-15 (10) catalyst [41].

The experiments conducted with sulfated and non-sulfated Ti-SBA-15 (10) catalysts with the Si/Ti ratio of 10, revealed that SO_4/Ti-SBA-15 (10) yielded more than three times epoxy canola oil conversion (100 %) than Ti-SBA-15 (10). Also, the largest amount of sulfur (2.1 %) and the highest amount of strong acid sites were achieved with SO_4/Ti-SBA-15 (10) catalyst, since the increase of Ti amount in the structure led to more sulfur binding to the structure and thus provided enhanced acidity. The reusability of the sulfated Ti-SBA-15(10) catalyst was tested four times.

Rashid et al. (2019) prepared SBA-15 mesoporous silica nanoparticles by the sol-gel technique, employing P123 surfactant and calcined at different temperatures to examine the influence of calcination on particle and surface structure [43]. Various calcination conditions were discovered to have a considerable impact on surface area and porosity. Silica calcined at 200 ^oC had essentially negligible porosity, whereas silica calcined at 300 ^oC begins to exhibit porous character with the removal of the P123 template. According to FT-IR analysis, silica calcined at 110 ^oC and 200 ^oC exhibited a characteristic surfactant band (2850-2950 cm^{-1}, 1730 cm^{-1}) that declines at 300 ^oC, suggesting partial elimination of the template, which results in a lower silica surface area and pore size. Silica calcined at 700 ^oC was reported to have a smaller surface area (315 m^2/g) and total pore volume (0.55 cm^3/g), than silica calcined at 500 ^oC (488 m^2/g and 0.74 cm^3/g, respectively), which might be attributed to the shrinking of SBA-15's damaged hexagonal pores. The calcination temperature of 500 ^oC was found to yield the best surface characteristics and porosity with the BET surface area of 641 m^2/g, total pore volume of 1.67 cm^3/g, and pore size of 7.5 nm.

Therefore, from the above studies, it can be concluded that the large surface area, mesoporosity, and high acidity of sulfated Ti-SBA-15(10) can yield the desired results in cellulose acetate production.

3.2.2. Sulfated TiO_2-SiO_2 Catalysts

Utilization of mixed metal oxides, bimetallic catalysts combined with promoters may offer better acidity and thermal stability than single oxides. Among the many mixed oxides, titania-silicates attracted much attention in recent years [44, 45, 46] due to the combination of TiO_2 and SiO_2 provided more acid sites generation than other mixed oxides [47, 45].

Acid sites on TiO_2-SiO_2 mixed oxide increase through the well-dispersed Ti atoms on SiO_2. The existence of Ti provides Lewis acid sites in the TiO_2-SiO_2 [44, 47]. Lewis acid sites have electron acceptor qualities, which allow reactions to take place via electron transfer or electron sharing by creating covalent bonds. The sulfur atoms and sulfate ions (SO_4^{2-}) create strong Brønsted acidity, which is created by the highly electronegative sulfate group polarization with the neighboring -OH groups [50].

Because of the weak interaction between a single metal oxide and sulfur, sulfur atoms in the structure leach rapidly. Preparing TiO_2-SiO_2 rather than just TiO_2 provides the formation of strong chelating bonds during calcination which reduce surface sulfur from leaching and improve stability [47], as given in Figure 3.9.

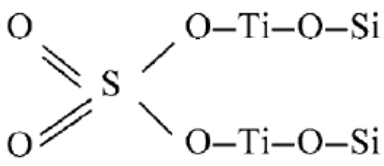

Figure 3.9. Chelating bidentate bonds in titania-silicates [47].

Yang et al. (2003) tested the effect of calcination temperature on SO_4/TiO_2-SiO_2 catalyst for acetic acid esterification with glycerin [47]. The mixed oxide was prepared by precipitation and then sulfated by impregnation of 1 M H_2SO_4. The resultant material

was calcined at various calcination temperatures. Among calcination temperatures of 400 °C to 600 °C; 450 °C was reported to be the optimum calcination temperature in terms of yielding the highest catalyst surface area (550 m^2/g). Due to sulfate decomposition, the specific surface area of a sample calcined at 600 °C was enhanced (594 m^2/g).

In the study of Shao et al. (2013), the synthesis of TiO_2-SiO_2 mixed oxides was carried out by the sol-gel method at 80 ^oC for the esterification of waste oil and oleic acid. Impregnation of sulfate group of 1 M H_2SO_4 on TiO_2-SiO_2 support was employed for the synthesis of SO_4/TiO_2-SiO_2 catalyst at room temperature. Four different calcination temperatures (450 ^oC, 550 ^oC, 650 ^oC, and 800 ^oC) were investigated since calcination temperature was reported as an important criterion in the literature studies for the sulfur content, pore structure, and surface area. Calcination at 450 °C yielded the largest catalyst surface area (457 m^2/g), pore volume (0.28 cm^3/g), the highest sulfur content (5.37 %), and conversion (77 %). The chelating bidentate bonds in TiO_2-SiO_2 are strong Brønsted sites that are formed around 400-450 ^oC during calcination [45].

Li et al. (2013), studied the catalytic activity and stability of lanthanum ion (La^{+3}) incorporation into the sulfated TiO_2-SiO_2 mixed oxide for the esterification of itaconic acid [44]. The TiO_2-SiO_2 catalyst was prepared by the sol-gel method. La_2O_3 was dissolved in 2 mol/L H_2SO_4 and TiO_2-SiO_2 was impregnated with this solution. Then the materials were calcined in air at 400-600 °C for 6 h. Brønsted and Lewis acid sites of La incorporated SO_4^{2-}/TiO_2-SiO_2 catalysts were identified by NH_3-FTIR, given in Figure 3.10. The inorganic bidentate SO_4^{2-} ions coordinated to TiO_2 were detectable at 800–1630 cm^{-1}. Below and at 550 °C calcination temperature, the peaks at 1400–1401 cm^{-1} and 1631–1632 cm^{-1} were associated with NH_3 adsorbed on Brønsted acid sites and Lewis acid sites, respectively. Above 550 °C it was observed that the Brønsted acid sites almost disappeared due to the high calcination temperature caused by the sulfate ion decomposition.

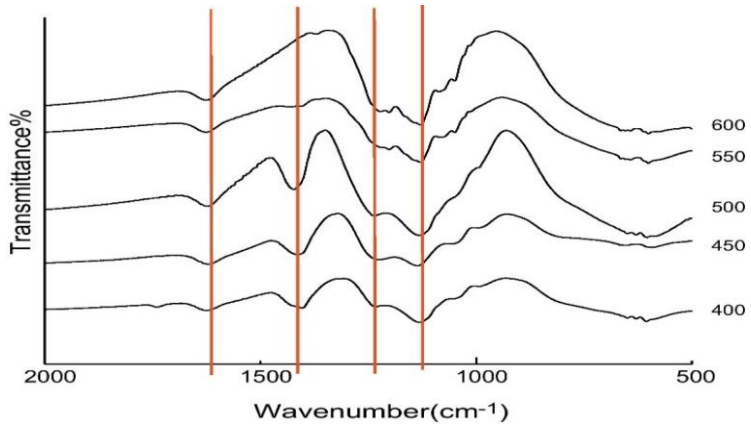

Figure 3.10. NH_3-FT-IR spectra of La incorporated $SO_4^{2-}/TiO_2–SiO_2$ at different calcination temperatures [44].

An anatase structure was observed by XRD analysis which reflects the highly dispersed Si and La on the catalyst. The incorporation of La^{+3} to the $SO_4^{2-}/TiO_2–SiO_2$ catalyst was observed to improve catalyst stability and allowed the attachment of sulfur groups to the surface. The enhancement in yield was also attributed to the increase in the number of acid sites. Even though methanol was utilized as a highly polar solvent, catalyst activity remained constant up to 8 times of reuse. Consequently, La incorporation to TiO_2-SiO_2 prevented the leaching of surface sulfur groups [44].

3.3. Assessment of Literature Studies

According to the literature studies, the cellulose acetate synthesis reactions should be carried out with heterogeneous catalysts having a high surface area, and large pore size [14, 37, 38]. Incorporating many advantages such as single pore size distribution, highly ordered pore channels, and large specific surface area, mesoporous molecular sieves such as MCM-41 and SBA-15 stand out as carriers. Among the mesoporous materials, SBA-15 has a specific surface area (600−1000 m^2/g), adjustable pore diameter (5−30 nm), and better hydrothermal stability than other mesoporous materials, which explains its more frequent preference in the literature [4, 14, 15]. The sulfate groups loaded on the acidic catalyst support create Brønsted acid sites that are responsible for the catalytic action. From the perspective of cellulose acetylation, Brønsted acid sites activate the acetic

anhydride molecules and thus facilitate the accessibility of acetyl groups to cellulose hydroxyl groups. As a result, the literature studies emphasize the importance of strong Brønsted acidic sites (SO_4^{2-}/–SO_3H) in the reaction. In this regard, sulfated Ti-SBA-15 and sulfated TiO_2-SiO_2 were considered as good candidates for the acetylation of cellulose in the present study.

Considering the literature studies on TiO_2-SiO_2 mixed oxides, sulfated TiO_2-SiO_2 (SO_4^{2-}/TiO_2-SiO_2) and La incorporated SO_4^{2-}/TiO_2-SiO_2 will be synthesized, and their stability and activity will be investigated on the cellulose acetate synthesis reaction. For higher amount of catalyst sulfate content, the calcination temperature of the sulfated catalyst will be selected as 450 °C, as reported by Shao et al. (2013) [45] and Yang et al. (2003) [47].

CHAPTER 4

EXPERIMENTAL STUDY

The study aimed to investigate the performance of 6 different synthesized catalysts, which were SO_4/Ti-SBA-15, SO_4/La-TiO_2-SiO_2, SO_4/TiO_2-SiO_2, CSA/Ti-SBA-15 (10), CSA/Ti-SBA-15 (6), and CSA/Ti-SBA-15 (20) for the cellulose acetylation reaction. For the most active, stable, and selective catalyst, different reaction parameters were changed to observe the effect of the reaction time and catalyst/microcrystalline cellulose weight ratio (0.1, 0.25, 0.50) on cellulose acetate formation. Catalyst leaching tests were performed to determine the catalyst stability. Reusability tests were conducted to understand the catalyst activity.

Ti incorporated SBA-15 silica materials with different loading amounts of titanium were synthesized. Ti-SBA-15 catalysts were prepared via hydrothermal synthesis by using gels with three different Si/Ti molar compositions, which were 6:1, 10:1, and 20:1. The catalysts were calcined at 550 °C. Sulfated forms of Ti-SBA-15 catalysts were prepared by two sulfate sources, which were chlorosulfonic acid and ammonium sulfate solution. According to the sulfate source, the catalysts were denoted as SO_4/Ti-SBA-15 and CSA/Ti-SBA-15. Lastly, the prepared catalysts were tested in the reaction.

La incorporated titania-silica (La-TiO_2-SiO_2) and titania-silica (TiO_2-SiO_2) catalysts were prepared by the sol-gel method. Lanthanum nitrate (La $(NO_3)_3$) was used as the La source. The calcination step was performed at 450 ^oC. Another sulfated TiO_2-SiO_2 catalyst was synthesized by the same procedure, however, no La $(NO_3)_3$ was not added to the mixture during the synthesis, to investigate the effect of La incorporation. TiO_2-SiO_2 catalysts were sulfated with 1 M of $(NH_4)_2SO_4$ per gram of catalyst for 1 hour. Finally, SO_4/TiO_2-SiO_2 and SO_4/La- TiO_2-SiO_2 catalysts were calcined at 450 °C for 6 h.

4.1. Materials

The chemicals used for the experimental study are given in Table 4.1.

Table 4.1. The chemicals used for the experimental study.

Chemical	**Brand/Purity**
Acetic anhydride	Acros Organics, 97+ %
Acetone	Sigma-Aldrich, ≥99.5 %
Amberlyst-15	Sigma-Aldrich, 216380
Ammonium sulfate solution	Isolab Chemicals, ≥ 99.5 %
Chloroform	Sigma-Aldrich, ≥ 99 %
Chlorosulfonic acid	Sigma-Aldrich, ≥ 99 %
Deuterated chloroform	Merck, 99.8 %
Dichloromethane	Sigma-Aldrich, ≥99.5 %
Ethanol	Sigma-Aldrich, ≥99.8
Hydrochloric acid	Sigma-Aldrich, 37 %
Microcrystalline cellulose	Sigma-Aldrich, (~50 μm)
Pluronic P123	Sigma-Aldrich, 435465
Sulfuric acid	Merck, 95-97 %
Tetraethyl orthosilicate	Sigma-Aldrich, ≥ 99.0 %
Titanium (IV) isopropoxide	Sigma-Aldrich, 97 %

4.2. Synthesis of Catalysts

The list of catalysts synthesized were given in Table 4.2.

Table 4.2. Labels of the prepared catalysts.

Catalyst	***Catalyst Specifics***
SO_4/TiO_2-SiO_2	1.0 M $(NH_4)_2SO_4$
SO_4/La-TiO_2-SiO_2	1.0 M $(NH_4)_2SO_4$, La/Si mole ratio: 0.01

Table 4.2. (cont'd) Labels of the prepared catalysts.

Catalyst	*Catalyst Specifics*
SO_4/Ti-SBA-15	1.0 M $(NH_4)_2SO_4$, Si/Ti mole ratio: 10
CSA/SBA-15	0.5 M HSO_3Cl
CSA/Ti-SBA-15 (6)	0.5 M HSO_3Cl, Si/Ti mole ratio: 6
CSA/Ti-SBA-15 (10)	0.5 M HSO_3Cl, Si/Ti mole ratio: 10
CSA/Ti-SBA-15 (20)	0.5 M HSO_3Cl, Si/Ti mole ratio: 20
W-CSA/Ti-SBA-15 (10)	0.5 M HSO_3Cl, Si/Ti mole ratio: 10, Refluxed with acetic anhydride (80 °C, 1 h)
WW-CSA/Ti-SBA-15 (10)	0.5 M HSO_3Cl, Si/Ti mole ratio: 10, Refluxed with acetic anhydride (80 °C, 1 h) & washed with DI water.
A-CSA/Ti-SBA-15 (10)	0.5 M HSO_3Cl, Si/Ti mole ratio: 10, Refluxed with acetone (60°C, 0.5 h) after the reaction.

4.2.1. Synthesis of SO_4/Ti-SBA-15 catalyst

Titanium incorporated SBA-15 catalysts were prepared by the hydrothermal method. For the synthesis of Ti-SBA-15 (Si/Ti mole ratio=10), 9.28 g of Pluronic P-123 was dissolved in 229 ml g of water by mechanical stirring at 40 °C for 2 h. Then, 4.54 g of HCl (37 %) was added to the mixture and left stirred for another 2 h. As the silica (Si) and Ti sources, 20.83 g tetraethyl orthosilicate (TEOS) and 2.84 g titanium isopropoxide (TISOP) were added dropwise, and the solution was stirred for 24 h at 40 °C. After, hydrothermal treatment of the resultant mixture was carried out in an autoclave at 100 °C for another 24 h by putting the mixture in a Teflon autoclave. For the separation of the solid phase, centrifugation was conducted by washing the solid three times with deionized water. The solid material was then dried overnight in a furnace at 100 °C. After grinding, it was then calcined under air at 550 °C for 6 h [46].

For the sulfation of Ti-SBA-15 (10), 1 M ammonium sulfate ($(NH_4)_2SO_4$) solution was used per gram of the catalyst. The sulfation was carried out at room temperature for 1 h, and after the catalyst is filtrated, it was calcined for 6 h at 450 °C. The sulfated catalyst was named as SO_4/Ti-SBA-15 (10).

4.2.2. Synthesis of SO_4/TiO_2-SiO_2 and SO_4/La-TiO_2-SiO_2 catalysts

La incorporated titania-silica (TiO_2-SiO_2) catalysts were prepared by the sol-gel method. For a sample synthesis, first, the hydrolysis of TEOS (6.6 ml) was carried out with 3.51 ml ethanol and 0.65 ml 0.05 M HCl (37 %) at room temperature for 1.5 h. Then, TISOP-isopropanol solution, (Ti/isopropanol mass ratio=1) was added dropwise. The La source 0.1 g lanthanum nitrate (La $(NO_3)_3$) was added and then the mixture was stirred until homogeneous (45 min). After 2.35 ml of deionized water was added, the solution was further stirred for 1 h. Dropwise addition of 1 M ammonia solution (NH_4OH) was carried out until a transparent gel formation was observed. The resultant gel was aged at room temperature overnight and then dried at 80 ^oC overnight. Before the calcination step at 500 ^oC for 4 h, the product was ground. Another sulfated TiO_2-SiO_2 catalyst was synthesized by the same procedure, however, no La $(NO_3)_3$ was not added to the mixture during the synthesis, to compare the effect of La incorporation.

TiO_2-SiO_2 catalysts were sulfated with 1 M of $(NH_4)_2SO_4$ per gram of catalyst for 1 h. Finally, SO_4/TiO_2-SiO_2 and SO_4/La- TiO_2-SiO_2 catalysts were calcined at 450 °C for 6 h.

4.2.3. Synthesis of CSA/Ti-SBA-15 and CSA/SBA-15 catalysts

Ti-SBA-15 (10) catalyst was synthesized according to the method explained in section 4.2.1. [46]. To investigate the effect of Ti metal amount on the catalyst, Ti-SBA-15 catalysts were prepared with three different Si/Ti mole ratios of 6, 10, and 20 by using chlorosulfonic acid as the sulfation agent. To synthesize Ti-SBA-15 with Si/Ti mole ratio of 20 and 6 (Ti-SBA-15 (20) and Ti-SBA-15 (6)), 1.42 g and 4.73 g of TISOP was used, instead of 2.84 g. Also, SBA-15 without TISOP addition was prepared to investigate the effect of Ti incorporation.

Sulfation of Ti-SBA-15 (6), Ti-SBA-15 (10), and Ti-SBA-15 (20) catalysts was carried out for 5 min, using 0.5 M of chlorosulfonic acid solution in methylene dichloride per gram of the catalyst. After the catalyst was filtrated, it was calcined at 450 ^oC for 6 h.

They were called CSA/Ti-SBA-15 (6), CSA/Ti-SBA-15 (10) and CSA/Ti-SBA-15 (20). The CSA/SBA-15 was also synthesized with the same procedure, except for TISOP addition.

4.3. Characterization of Catalysts

In this study, N_2 adsorption-desorption (BET), X-Ray Diffraction (XRD), X-Ray Fluorescence (XRF), FT-IR spectroscopy, temperature-programmed desorption of ammonia (NH_3-TPD), and thermogravimetric analysis (TGA) were performed. The analysis details are given in the following sections. As a result of these analyzes, the following information about the catalysts was obtained: thermal stability, the chemical bonds and groups in the structure, crystallinity, acidity, surface area, pore size, and the ratio of elements and compounds in its structure.

4.3.1. Nitrogen Adsorption-Desorption (BET)

The nitrogen physisorption studies were performed by Micromeritics ASAP 2010 model static volumetric adsorption instrument. Before adsorption experiments, the catalysts were degassed at 200°C for 6 h. Nitrogen adsorption was carried out at 77 K.

4.3.2. X-Ray Diffraction (XRD)

To investigate the crystalline regions of the catalysts, a Philips X'Pert diffractometer with a Cu-Kα radiation source was used. With a step length of 0.02, the scattering angle 2θ was changed between 5° and 80°.

4.3.3. X-Ray Fluorescence (XRF)

To determine the elemental composition of the fresh and used catalysts, the X-Ray Fluorescence technique was carried out by using a Spectro IQ II instrument with Cu-Kα radiation.

4.3.4. Temperature Programmed Desorption of Ammonia (NH_3-TPD)

For the determination of acidic strength and total acidity of the catalysts, the temperature-programmed desorption of ammonia (NH_3-TPD) method was applied by Micromeritics AutoChem II Chemisorption Analyzer. The acid sites are divided into 3 as weak (25 °C-200 °C), moderate (200 °C-400 °C), and strong (> 400 °C) acid sites [58].

The catalyst samples were heated up to 500 °C with a heating rate of 5 °C/min and were kept for 1 h at this temperature under He gas flow (70 ml/min). Then, at a rate of 5 °C/min under He gas flow (30 ml/min), the sample was cooled to 90 °C. Then the flow was switched to NH_3-He gas mixture (30 ml/min) for 30 min. For the removal of physically adsorbed ammonia, the sample was degassed for 2 h under He flow (70 ml/min). Finally, for the desorption of ammonia, the sample was heated from 90 °C to 600 °C with a 10 °C/min heating rate.

4.3.5. Fourier Transform Infrared Spectroscopy (FT-IR) Spectroscopy

The characterization of catalyst framework vibrations was performed with a Shimadzu FTIR 8400S model spectrometer at room temperature between 400 and 2000 cm^{-1} wavenumbers and a resolution of 4 cm^{-1}. The KBr pellet method was used, and catalyst samples were prepared by pressing a 3 mg sample together with 150 mg KBr.

4.3.6. Thermogravimetric Analysis (TGA)

To examine the thermal stability of the catalysts in terms of weight loss, thermogravimetric analysis was performed by Shimadzu TGA-51 instrument using a heating sequence from room temperature to 800 ^{o}C at a ramp rate of 5 ^{o}C/min under flowing air.

4.3.7. Reusability

The catalytic reactions were repeated using the recycled catalyst and the same reaction conditions as the previous run. After being separated by centrifugation, the used catalyst was refluxed with acetone and then was dried at 120 °C for 3 h. The catalyst reuse experiments were carried out under the same reaction conditions.

4.4. Synthesis of Cellulose Acetate

The activity tests of the catalysts were conducted both for homogeneous and heterogeneous catalysts. Sulfuric acid was used as the homogeneous catalyst in the reaction and the reactions were carried out in a 100 ml glass reactor. 2 g of MCC, 5 g of acetic anhydride, 30 ml dichloromethane, and 0.04 g of H_2SO_4 were used in the reaction, which was conducted at 80°C for 4 h [31].

The production of cellulose acetate with acetalization reaction of cellulose was carried out with 6 different catalysts, which are SO_4/Ti-SBA-15, SO_4/La-TiO_2-SiO_2, SO_4/TiO_2-SiO_2, CSA/Ti-SBA-15 (6), CSA/Ti-SBA-15 (10), and CSA/Ti-SBA-15 (20). The acetic anhydride amount was determined by taking the molar ratio of acetic anhydride to cellulose anhydroglucose unit (n_{AA}/n_{AGU}) as 10:1. The heterogeneous reaction system consists of two necked round-bottom glass flask (50 ml), a magnetic stirrer, a condenser, and a heating mantle as shown in Figure 4.1.

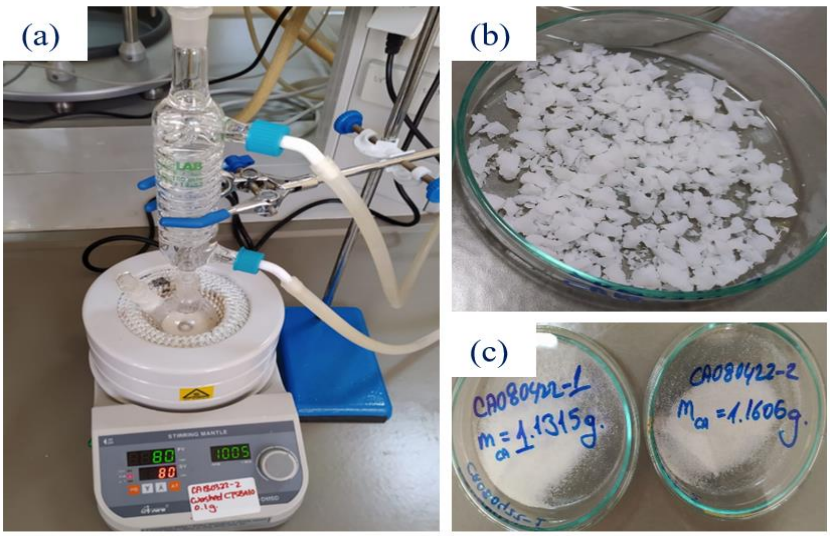

Figure 4.1. (a) Experimental set-up (b) cellulose acetate after filtration (c) dried and grinded cellulose acetate.

Firstly, a 50 ml round-bottom glass reactor equipped with a condenser was placed in the heating mantle, which provides heating and mechanical stirring. Then, 5.792 ml acetic anhydride and 1 g vacuum dried (24 h) microcrystalline cellulose (n_{AA}/n_{AGU} =10:1) were added to the flask and the mantle was adjusted to 80 °C and 1000 rpm. After reaching around 65 °C, the catalyst was added to the glass reactor. Because the reaction is exothermic, the temperature will rise quickly in the next 10-15 min. After the process temperature reaches equilibrium at 80 °C, the mantle temperature was set to 80°C and the reaction was allowed to proceed for 6 h. Figure 4.2 illustrates the cellulose esterification reaction.

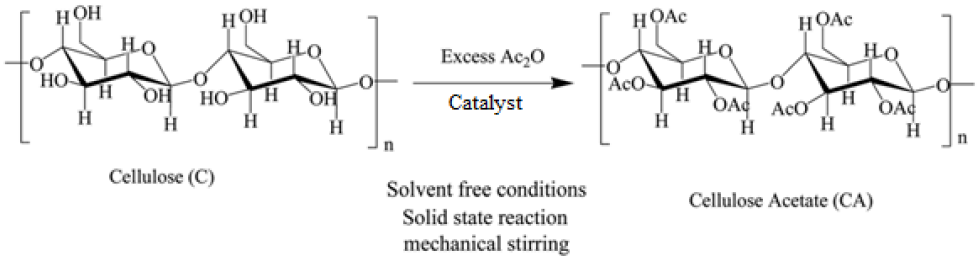

Figure 4.2. Esterification of cellulose with acetic anhydride to cellulose acetate.

The viscous product and catalyst liquid mixture obtained at the end of the reaction were allowed to cool to room temperature and then was diluted with 40 ml acetone. For

the product separation from the catalyst particles, the mixture was centrifuged at 4000 rpm for 10 min. To precipitate CA, the resulting transparent liquid was poured into 50 ml of 50 % (v/v) aqueous ethanol and stirred for 30 min. CA is filtered, and the excess acetic anhydride and acetic acid formed during the reaction were removed by deionized water during filtration. Finally, CA is vacuum dried overnight at 70 ^{o}C and then weighed.

For comparison, the reaction tests were also carried out with commercial Amberlyst-15 acidic catalyst and sulfuric acid under identical reaction conditions. As the homogeneous catalyst, 0.04 g H_2SO_4 was added to the reaction medium [31].

4.5. Characterization of Cellulose Acetate

Cellulose acetate samples were centrifuged, washed, filtered, and dried before being used for the analysis. As a result, the samples were purified of any leftover catalyst and impurities. Analysis of the samples was performed by proton Nuclear Magnetic Resonance (^{1}H-NMR spectroscopy), FT-IR, and thermogravimetric analysis (TGA). As the solvent for the ^{1}H-NMR spectroscopy, deuterated chloroform ($CDCl_3$) was employed.

4.5.1. Yield

The catalytic performance was measured in terms of isolated product yield and degree of substitution (DS) value. Using the formula proposed by Fan et al. (2014) [11], the isolated product yields were calculated based on the complete cellulose acetylation.

$$\text{Yield (\%)} = \frac{\text{Actual yield of CA (g)}}{\text{Theoretical yield of CA (g)}} = \frac{m_{CA}}{m_C \text{ x } 162/291} \text{ x } 100$$

where, m_{CA} , m_C , 162, and 291 are; the mass of CA, the mass of cellulose, the mass of anhydroglucose unit (AGU) of cellulose (g/mol), and the mass of cellulose triacetate (CA) (g/mol) respectively.

4.5.2. ^{1}H-NMR Spectroscopy

The degree of substitution of the cellulose acetate samples was determined from ^{1}H-NMR data by analyzing the peaks of methyl proton and cellulose AGU unit by using the given equation [48, 49]. $A_{Acetate}$ (1.5–2.3 ppm) refers to the area of the methyl proton signals and A_{AGU} (3.5–5.8 ppm) is the area of the proton signals of the cellulose AGU unit.

$$DS = \frac{7 \text{ x } A_{Acetate}}{3 \text{ x } A_{AGU}}$$

CA samples were analyzed by Varian Inova 300 MHz spectrometer instrument using deuterated chloroform ($CDCl_3$) as the solvent and TMS as an internal standard. For the analysis, 10 mg of CA was dissolved in 0.6 ml of $CDCl_3$. Then, the resultant solution was put into a 5 mm diameter glass NMR tube. The number of scans used was 32.

4.5.3. FT-IR Analysis

The obtained CA products Swere analyzed by Shimadzu FTIR 8400S model spectrometer, to observe the characteristic of C=O acetate peak and -OH stretching signals from the FT-IR patterns.

4.5.4. Thermogravimetric Analysis (TGA)

Thermogravimetric measurement has been used to evaluate the thermal characteristics of native microcrystalline cellulose and cellulose acetate Shimadzu TGA-51 equipment under the N_2 environment with a heating rate of 10 ^{o}C/min.

CHAPTER 5

RESULTS AND DISCUSSION

5.1. Characterization of the Catalysts

The morphological and chemical characteristics of the catalysts have significant effect on the reaction and product formed. Thus, investigation of catalysts is critical to predict their activity in the reaction. The following analyses were performed for the catalyst characterization: TGA, FT-IR Spectroscopy, XRD, NH_3-TPD, N_2 adsorption-desorption, and XRF. Through these analyses, information about the catalysts' thermal stability, chemical bonds and groups in its structure, crystallinity, acidity, surface area, pore size, the elements, and compounds in its structure was obtained.

5.1.1. SO_4/Ti-SBA-15 Catalyst

The morphological properties of SO_4/Ti-SBA-15 catalyst were investigated by N_2 adsorption-desorption analysis. Figure 5.1 illustrates the N_2 adsorption isotherm of SO_4/Ti-SBA-15. The sample exhibits type IV adsorption/desorption isotherm, indicating a mesoporous structure. Also, the isotherm indicates a type H1 hysteresis loop, which is associated with cylindrical pores [51].

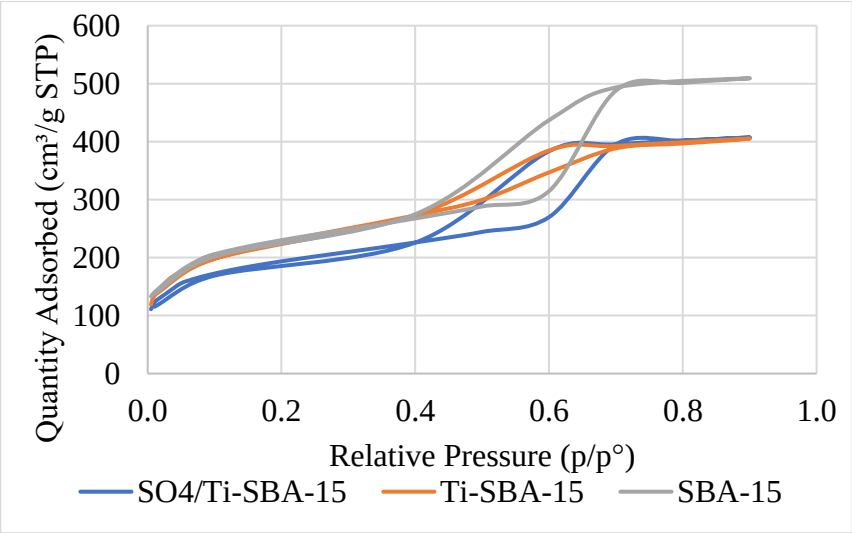

Figure 5.1. Nitrogen adsorption/desorption isotherm of SO_4/Ti-SBA-15.

According to the N_2 adsorption-desorption results, it was observed that sulfation of Ti-SBA-15 decreased the BET surface area from 778.5 m^2/g to 647.3 m^2/g as shown in Table 5.1. This was attributed to the formation of sulfate linkage [41]. The Ti incorporation slightly increased the BET surface area. The specific surface area, mean pore volume, and pore diameter of SO_4/Ti-SBA-15 catalyst were found as 647.3 m^2/g, 0.49 cm^3/g, and 4.5 nm, respectively.

Table 5.1. Morphological properties of Ti-SBA-15 and SO_4/Ti-SBA-15 catalysts.

Catalyst	S_{BET} (m^2/ g)	Pore Volume (cm^3/g)	Pore Size (Å)
SBA-15	766.8	0.63	47.8
Ti-SBA-15	778.5	0.45	35.3
SO_4/Ti-SBA-15	647.3	0.49	45.1

According to XRD graph illustrated in Figure 5.2, the amorphous SiO_2 structure of Ti-SBA-15 catalyst can be observed. Also, the peaks at $2\theta = 25.5^o$, 38^o, 48^o and 53^o indicate the presence of anatase titanium for Ti-SBA-15 catalyst. The absence of the mentioned peaks in SO_4/Ti-SBA-15 indicate the homogenous distribution of TiO_2 in the catalyst structure. [52, 46].

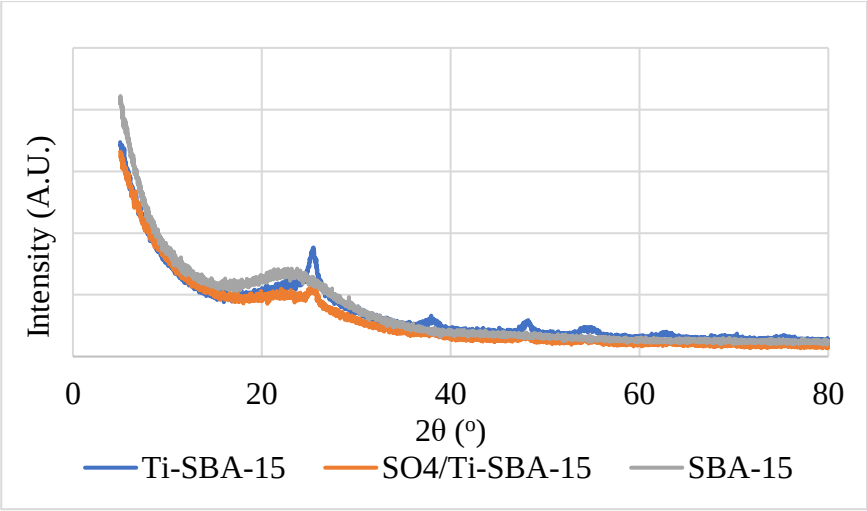

Figure 5.2. XRD results of SBA-15, Ti-SBA-15, and SO_4/Ti-SBA-15.

FTIR spectra of Ti-SBA-15 and SO_4/Ti-SBA-15 were given in Figure 5.3. The peaks at 800 and 1085 cm^{-1} correspond to symmetrical and asymmetrical Si-O-Si bonds, respectively. At 952 cm^{-1}, Ti-O-Si vibrations were observed. Generally, the peak range of sulfate bend peak is between 450-610 cm^{-1} and stretching sulfate group is between 980 and 1100 cm^{-1} [53]. The highly intense peak at 1085 cm^{-1} is due to overlapping of the sulfated group and Si-O-Si vibrations [45]. Therefore, the symmetric S=O stretching and asymmetric S-O stretching bonds could not be observed. Between 3300-3700 cm^{-1}, surface hydroxy group and physisorbed water due to sulfation were observed [41, 54].

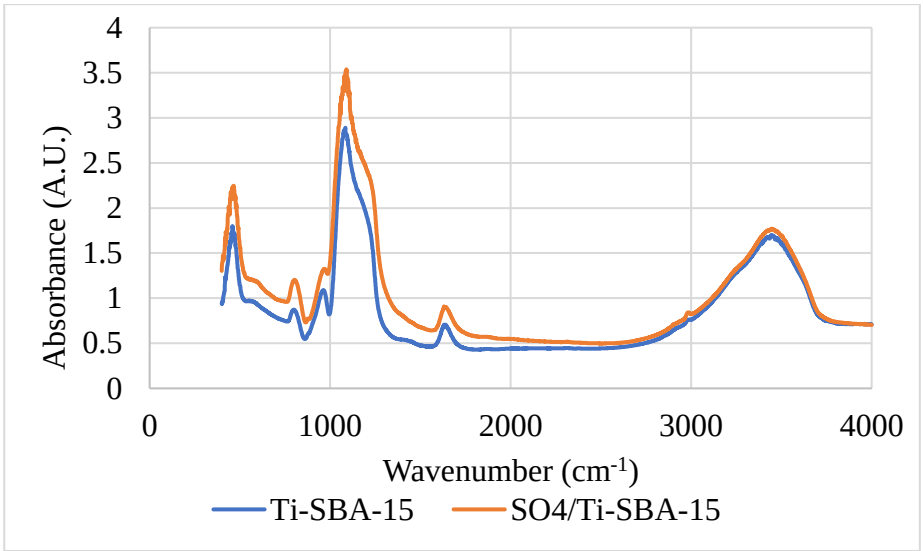

Figure 5.3. FT-IR results of Ti-SBA-15 and SO_4/Ti-SBA-15.

NH_3-TPD results in Figure 5.4 illustrates that SO_4/Ti-SBA-15 had high acidity with weak (130 °C-200 °C), moderate (200 °C-400) and strong (> 400 °C) acid sites. On the other hand, Ti-SBA-15 catalyst had low acidity. The acidities of Ti-SBA-15 (10) and SO_4/Ti-SBA-15 (10) catalysts were found as 0.558 and 3.795 mmol NH_3/gcatalyst, respectively. Sulfation increased the acidity significantly.

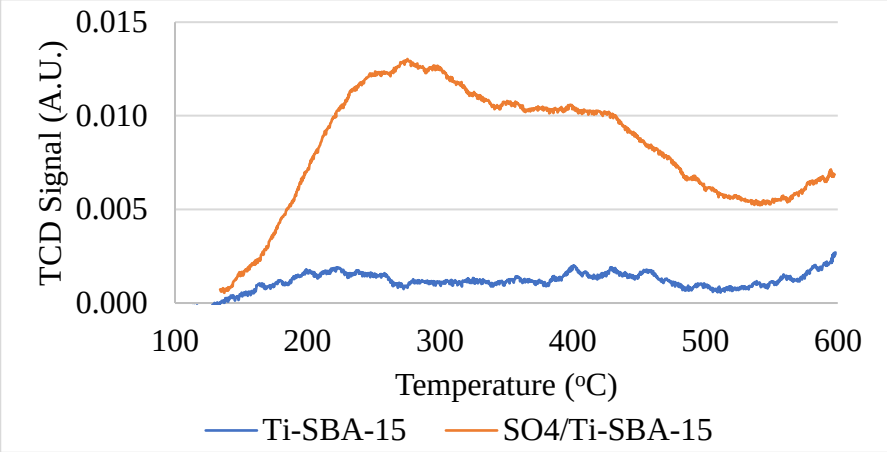

Figure 5.4. NH_3-TPD results of Ti-SBA-15 and SO_4/Ti-SBA-15 catalysts.

According to TGA results (Figure 5.5), it was observed that water removal occurs in both sulfated and sulfate-free Ti-SBA-15 catalysts up to 100 °C. In sulfate-free Ti-SBA-15 catalyst, there is no significant mass change at temperatures above 100 °C. In SO_4/Ti-SBA-15 catalyst, the decrease in the sample weight after 500 °C was attributed to sulfate decomposition.

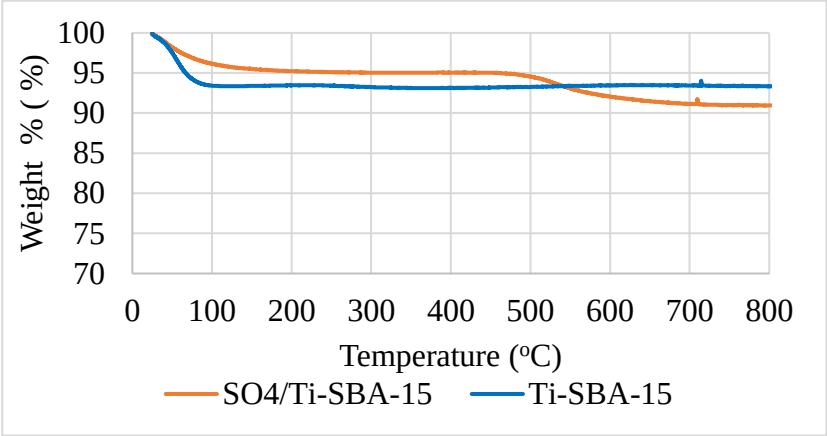

Figure 5.5. TGA analysis of Ti-SBA-15 and SO_4/Ti-SBA-15.

5.1.2. $SO_4/La\text{-}TiO_2\text{-}SiO_2$ and $SO_4/TiO_2\text{-}SiO_2$ Catalysts

The effect of the La incorporation and sulfation on the morphological properties of the TiO_2-SiO_2 catalysts were investigated. The N_2 adsorption-desorption isotherms of SO_4/TiO_2-SiO_2, TiO_2-SiO_2, and SO_4/La-TiO_2-SiO_2 catalysts were illustrated in Figure 5.6. It was observed that the catalysts exhibited mesoporous structure and narrow slit like pores due to type IV BET isotherm and narrow H4 hysteresis loops [52].

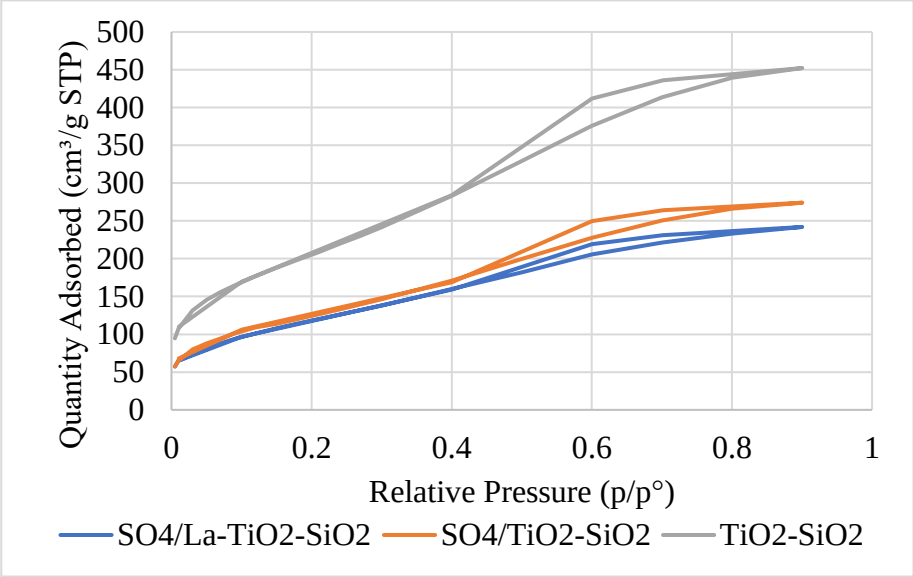

Figure 5.6. Nitrogen adsorption/desorption isotherms of SO_4/TiO_2-SiO_2, TiO_2-SiO_2, and SO_4/La-TiO_2-SiO_2 catalysts.

The morphological properties of the catalysts given in Table 5.2 show that catalysts have pores larger than 2.9 nm, indicating their mesoporous nature. It was observed that the La incorporation had effect on the pore size, and it decreased pore size from 39.8 Å to 33.4 Å. Similarly, pore volume decreased. Also, La addition to the TiO_2-SiO_2 caused the BET surface area to decrease. Sulfation of TiO_2-SiO_2 reduced surface area from 691 m^2/g to 462 m^2/g. Similarly, SO_4/La-TiO_2-SiO_2 had about 25 % lower BET surface area than non-sulfated La-TiO_2-SiO_2. This decrease in the catalyst surface area was attributed to the formation of sulfate linkages.

Table 5.2. Morphological properties of $SO_4/La\text{-}TiO_2\text{-}SiO_2$ and $SO_4/TiO_2\text{-}SiO_2$.

Catalyst	S_{BET} (m^2/ g)	Pore Volume (cm^3/g)	Pore Size (Å)
$TiO_2\text{-}SiO_2$	691.7	0.63	39.8
$SO_4/TiO_2\text{-}SiO_2$	462.2	0.35	34.3
$La\text{-}TiO_2\text{-}SiO_2$	591.2	0.36	33.4
$SO_4/La\text{-}TiO_2\text{-}SiO_2$	440.5	0.29	33.5

FT-IR spectra of $SO_4/TiO_2\text{-}SiO_2$ and $SO_4/La\text{-}TiO_2\text{-}SiO_2$ were given in Figure 5.7. Si-O-Si bending vibrations and symmetric stretching vibrations were observed at the peaks of 457 cm^{-1} and 811 cm^{-1}. The large peaks at 1100 cm^{-1} in both catalysts were attributed to the overlapped peaks of the asymmetrical Si-O-Si stretching and sulfate group vibration [45]. The small peak around 940 cm^{-1} in both catalysts was attributed to Si-O-Ti linkages [52]. The surface hydroxy group and physisorbed water were observed between 3000- 3700 cm^{-1} [46].

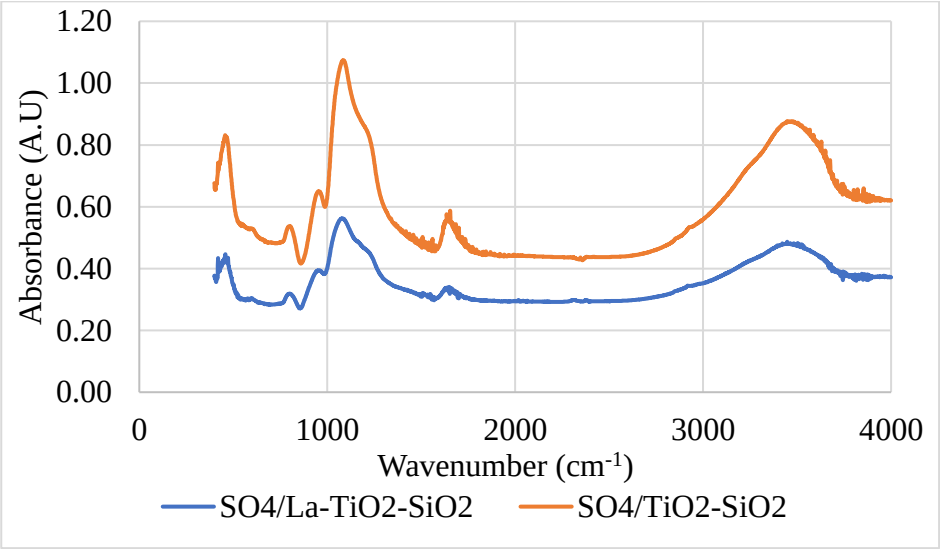

Figure 5.7. FT-IR results of $SO_4/TiO_2\text{-}SiO_2$ and $SO_4/La\text{-}TiO_2\text{-}SiO_2$.

NH_3-TPD analysis of $La\text{-}TiO_2\text{-}SiO_2$ and $SO_4/La\text{-}TiO_2\text{-}SiO_2$ catalysts are illustrated in Figure 5.8. Weak (100 ^oC-200 ^oC) and moderate acid sites between (200 ^oC-350 ^oC) were observed for $La\text{-}TiO_2\text{-}SiO_2$ catalyst which had an acidity of 1.634 mmol

NH_3/gcatalyst. Sulfation of La-TiO_2-SiO_2 catalyst increased the moderate and strong acid sites. This catalyst had an acidity of 3.319 mmol NH_3/gcatalyst.

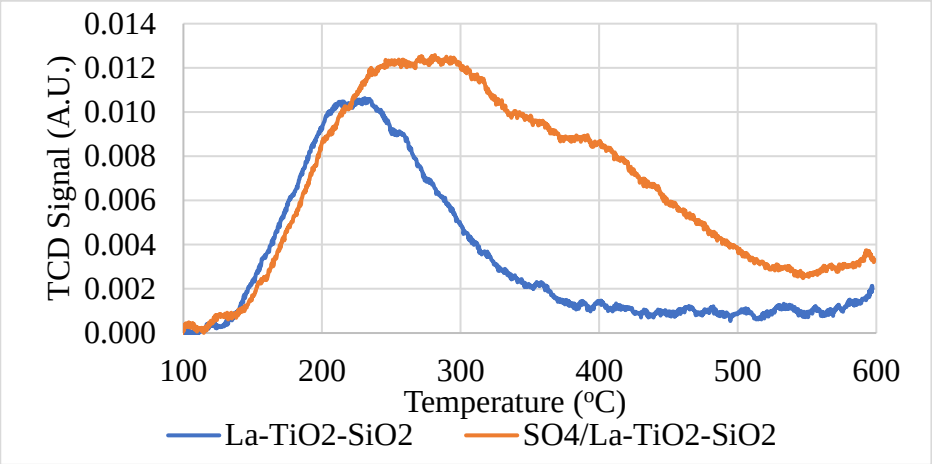

Figure 5.8. NH_3-TPD results of SO_4/La-TiO_2-SiO_2 and La-TiO_2-SiO_2.

NH_3-TPD analysis of TiO_2-SiO_2 and SO_4/TiO_2-SiO_2 catalysts were illustrated in Figure 5.9. Both weak (100 ºC-200 ºC), moderate (200 °C-400 °C), and strong (> 400 °C) acid sites were observed in TiO_2-SiO_2 catalyst with the acidity of 1.704 mmol NH_3/gcatalyst. Sulfation of TiO_2-SiO_2 catalyst demonstrates the increase in the moderate (200 °C-400 °C), and strong (> 400 °C) acid sites with the acidity of 3.198 mmol NH_3/gcatalyst.

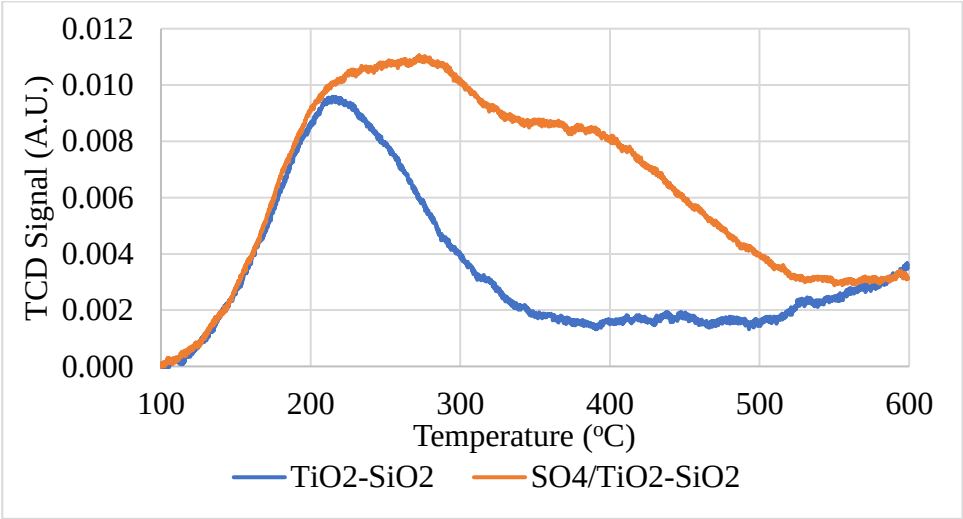

Figure 5.9. NH_3-TPD results of SO_4/TiO_2-SiO_2 and TiO_2-SiO_2.

XRD graphs in Figure 5.10 and Figure 5.11 indicate the presence of amorphous SiO_2 structure at $2\theta = 22^o$. Also, the homogenous distribution of TiO_2 in the amorphous silica was observed both in Figure 5.10 and Figure 5.11, due to absence of the peaks at $2\theta = 25.5^o$, 37^o, 48^o and 53^o [52]. In addition, high dispersion of La and Ti were noticed in La-TiO_2-SiO_2 and SO_4/La-TiO_2-SiO_2 catalysts due to the absence of La and Ti diffraction peaks.

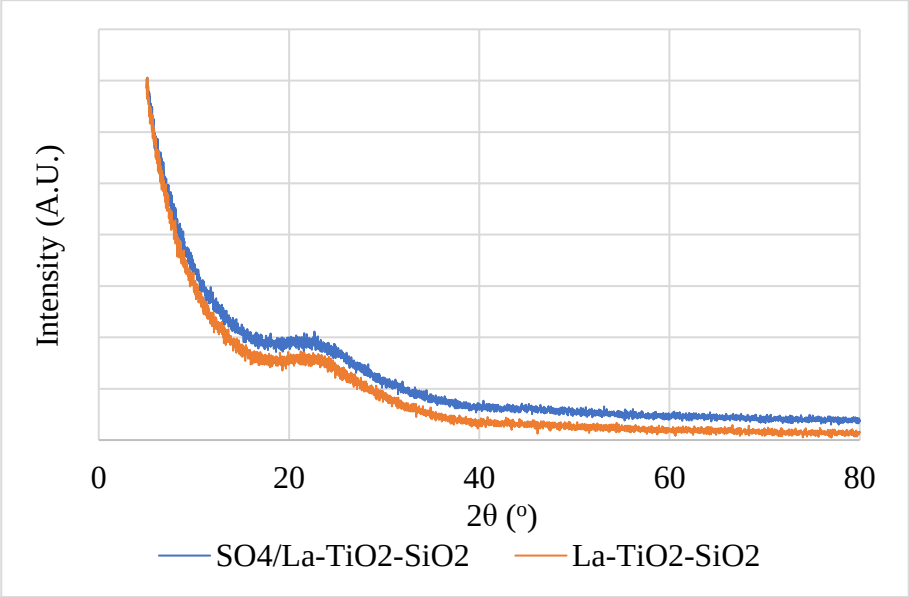

Figure 5.10. XRD analysis of SO_4/La-TiO_2-SiO_2 and La-TiO_2-SiO_2.

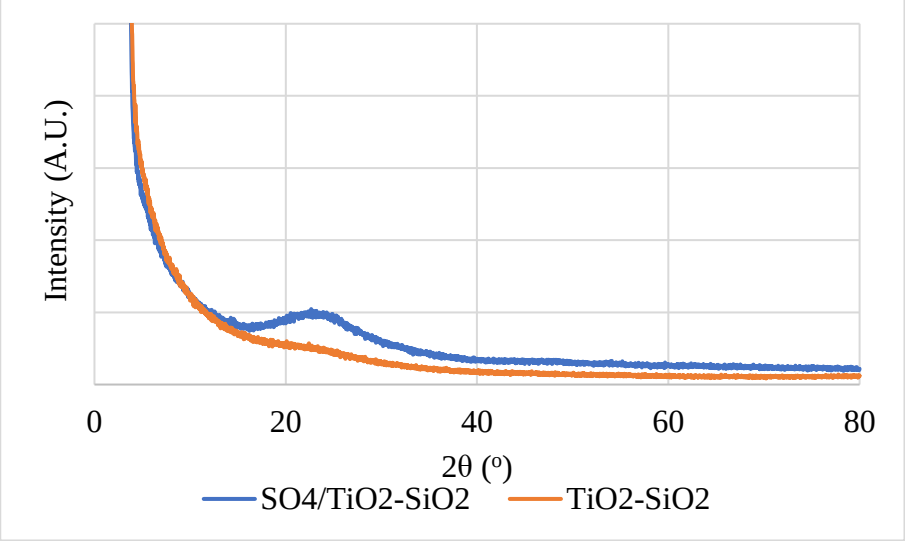

Figure 5.11. XRD analysis of SO_4/TiO_2-SiO_2 and TiO_2-SiO_2.

Thermal stability of the catalysts was investigated by TGA analysis, as given in Figure 5.12 and Figure 5.13. From room temperature to around 200 ºC, about 5 % of water with impurities were lost from the surface of the catalyst. After 450 ºC, which is the calcination temperature, about 4 % decrease in the weight was observed due to decomposition of sulfate groups. Ti sites attached to OH groups were detached from the surface after 700 ºC. Therefore, after 450 ºC, both the degradation of sulfate groups and the removal of structural hydroxyl were observed on the catalyst surface [52]. La addition was observed to increase the thermal stability of the catalysts.

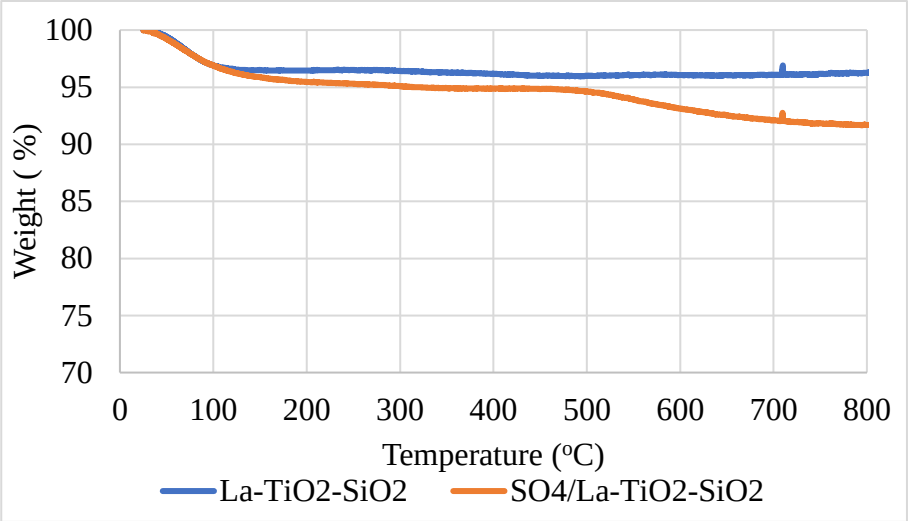

Figure 5.12. TGA results of SO_4/La-TiO_2-SiO_2 and La-TiO_2-SiO_2.

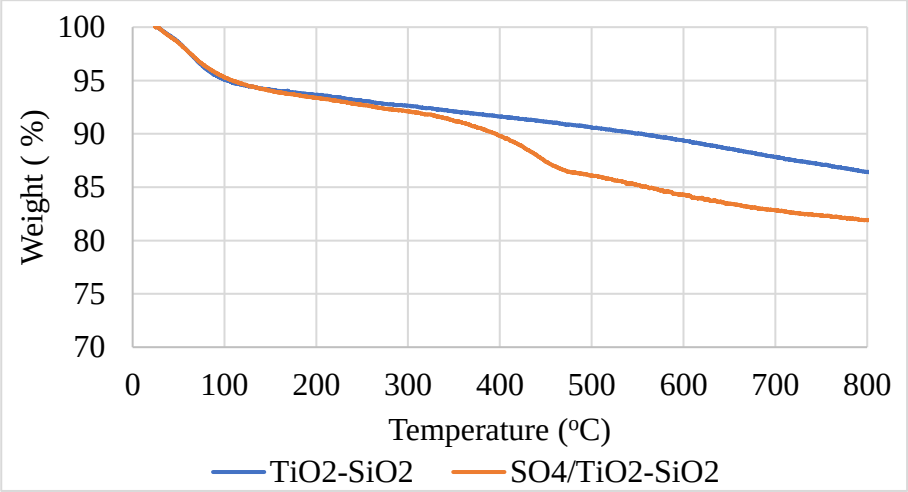

Figure 5.13. TGA results of SO_4/TiO_2-SiO_2 and TiO_2-SiO_2.

XRF results of the SO_4/TiO_2-SiO_2 and SO_4/La-TiO_2-SiO_2 catalysts were given in Table 5.3. It was observed that the addition of La to the structure resulted in approximately 53 % more sulfur binding to the surface, which was found to be compatible with the literature [44]. The fact that more sulfate groups were attached to the La-containing SO_4/La-TiO_2-SiO_2 catalyst increased the acidity.

Table 5.3. XRF result of the SO_4/TiO_2-SiO_2 and SO_4/La-TiO_2-SiO_2 catalysts.

Catalyst	S Content (%)	La Content (%)	Ti Content (%)	Si Content (%)
SO_4/TiO_2-SiO_2	0.449	10^{-3}	6.93	40.4
SO_4/La-TiO_2-SiO_2	0.687	2.43	6.44	38.9

5.1.3. CSA/Ti-SBA-15 and CSA/SBA-15 Catalysts

The effect of three different Si/Ti mole ratios (6, 10, 20) on the morphology of CSA/Ti-SBA-15 catalyst were investigated. The N_2 adsorption-desorption isotherms of CSA/Ti-SBA-15 (6), CSA/Ti-SBA-15 (10), and CSA/Ti-SBA-15 (20) catalysts were illustrated in Figure 5.14. All the catalysts were observed to have mesoporous structure, type IV BET isotherm and H1 hysteresis loops [52].

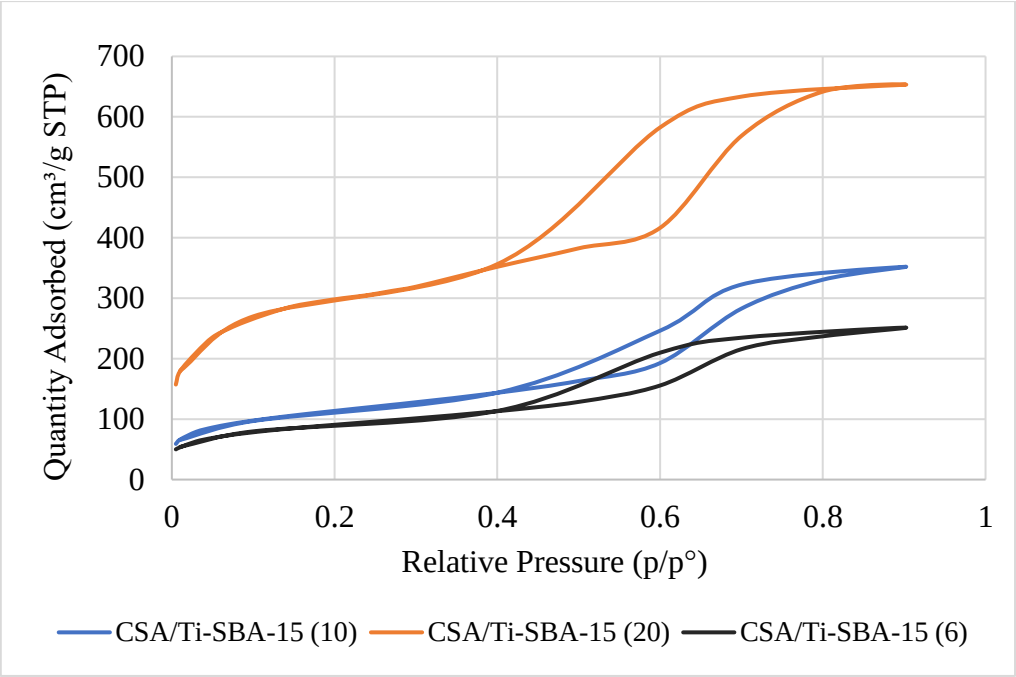

Figure 5.14. BET isotherms of CSA/Ti-SBA-15 catalysts.

BET results of CSA/Ti-SBA-15 catalysts were given in Table 5.4. Considering the BET results, as the Si/Ti mole ratio increased from 6 to 20, the BET surface area and pore volume increased since the catalyst contained less Ti in the structure. As expected, the catalyst with the highest Si/Ti mole ratio of 20 had given the largest BET surface area and pore volume of 1028 m^2/g and 0.76 cm^3/g, respectively. More Ti incorporation to SBA-15 resulted in lower pore volume and BET surface area.

Table 5.4. BET results of CSA/Ti-SBA-15 catalysts.

Catalyst	S_{BET} (m^2/g)	Pore Volume (cm^3/g)	Pore Size (Å)
CSA/Ti-SBA-15 (6)	315.23	0.34	47.18
CSA/Ti-SBA-15 (10)	398.18	0.49	50.50
CSA/Ti-SBA-15 (20)	1028.32	0.76	45.67

XRD patterns of Ti-SBA-15, CSA/Ti-SBA-15 (6), CSA/Ti-SBA-15 (10), and CSA/Ti-SBA-15 (20) were given in Figure 5.15. The peaks at 2θ of 25.5, 37.4, 48 and 53° observed for Ti-SBA-15 indicated presence of anatase titanium in the structure.

Sulfation with chlorosulfonic acid provided the homogeneous Ti distribution in the structure. The CSA/Ti-SBA-15 catalysts' structure had amorphous silica, as noticed from the characteristic broad peak at 2θ =22 °.

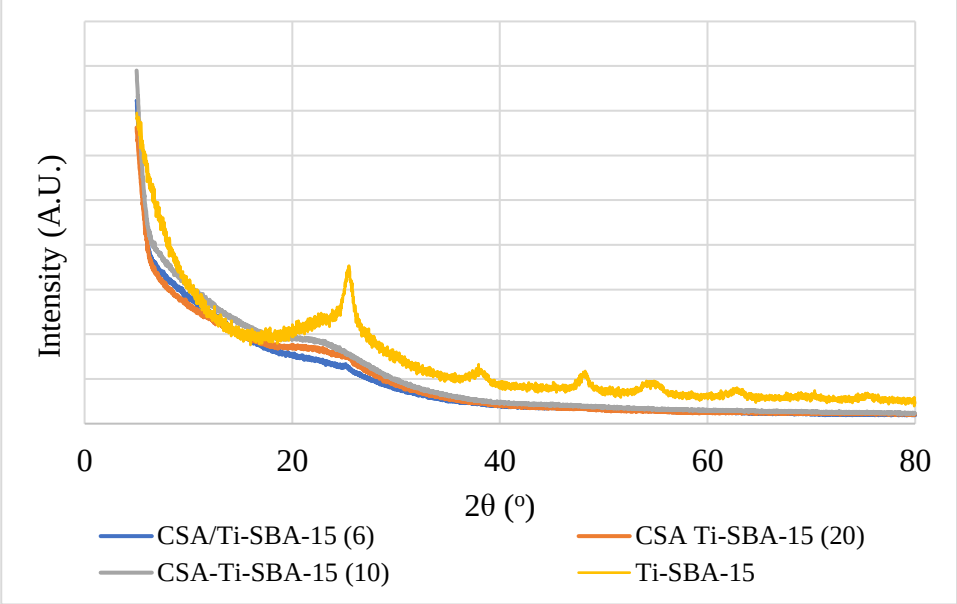

Figure 5.15. XRD graphs of CSA/Ti-SBA-15 catalysts.

Figure 5.16 represents the FTIR analysis of CSA/Ti-SBA-15 (6), CSA/Ti-SBA-15 (10), and CSA/Ti-SBA-15 (20) catalysts. The peaks observed at 462 cm^{-1} and 788 cm^{-1} were due to the Si-O-Si bending vibrations and symmetric stretching vibrations respectively. The overlap of the asymmetrical Si-O-Si stretching, and sulfate group vibration peaks can be seen at 1080 cm^{-1} [45]. Si-O-Ti bond peaks were observed around 971 cm^{-1} in all the catalysts [52]. The band around 1654 cm^{-1} is the result of the vibration of the adsorbed water molecule. Between 3000-3700 cm^{-1}, the peak due to surface hydroxy group and physisorbed water was observed. [46].

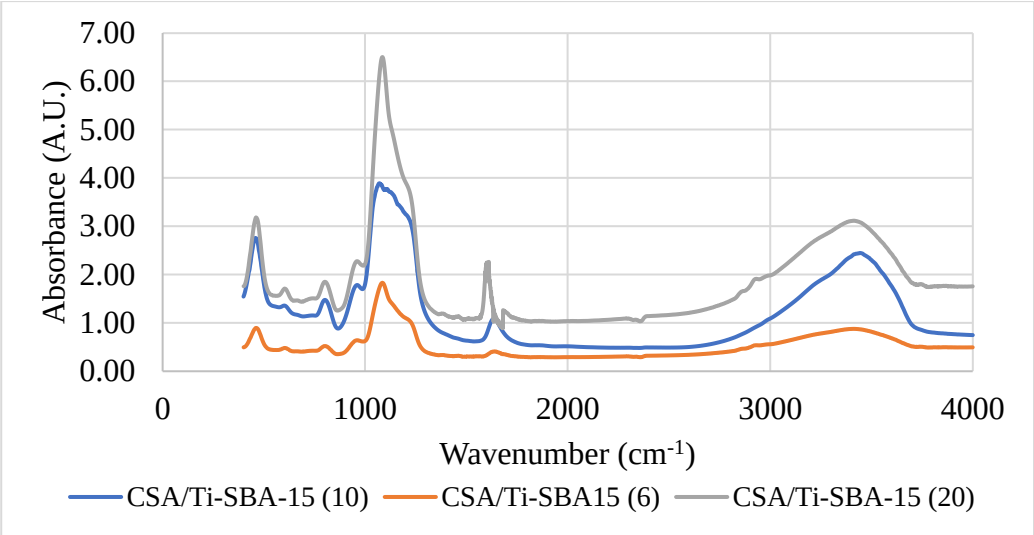

Figure 5.16. FT-IR results of CSA/Ti-SBA-15 catalysts.

NH_3-TPD analysis of CSA/Ti-SBA-15 (6), CSA/Ti-SBA-15 (10), and CSA/Ti-SBA-15 (20) catalysts were illustrated in Figure 5.17. A wide range desorption peak was observed showing that all the catalysts had weak (100 °C-200 °C), moderate (200 °C-400 °C), and strong (400 °C-550 °C) acid sites. With increase in Ti amount in the catalyst, the acidity was enhanced. CSA/Ti-SBA-15 catalysts' acidities are as follows: 1.613 mmol NH_3/gcatalyst for Si/Ti = 20, 3.844 mmol NH_3/gcatalyst for Si/Ti = 10 to 4.895 mmol NH_3/gcatalyst for Si/Ti = 6, respectively.

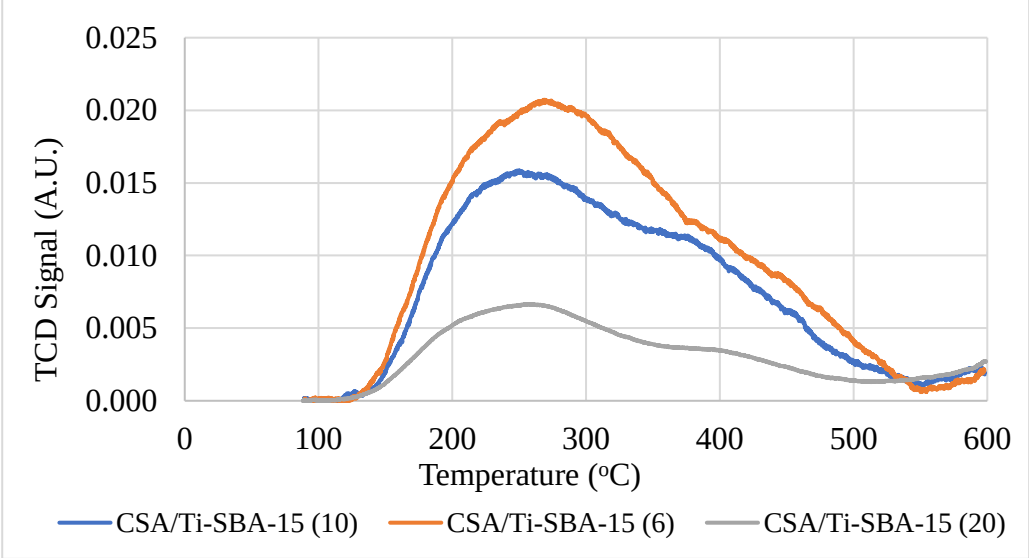

Figure 5.17. NH_3-TPD results of CSA/Ti-SBA-15 catalysts.

The thermal stability of CSA/Ti-SBA-15 (6), CSA/Ti-SBA-15 (10), and CSA/Ti-SBA-15 (20) catalysts was investigated and given Figure 5.18. Thermal stability of the catalysts was affected by the loss of adsorbed water between 25 °C and 150 °C. Second mass loss was observed to occur around 550 °C, which was attributed to the decomposition of sulfate groups. The comparison of tree catalysts indicated that the most thermally stable catalyst was found to be CSA/Ti-SBA-15 (10) with a Si/Ti mole ratio of 10. Compared to other CSA/Ti-SBA-15 catalysts, some parts of the excess Ti groups on the surface of this catalyst were attached to the surface by weak physical bonds. Therefore, the least stable catalyst was CSA/Ti-SBA-15 (6), and the highest amount of sulfate group decomposition was observed at 550 °C.

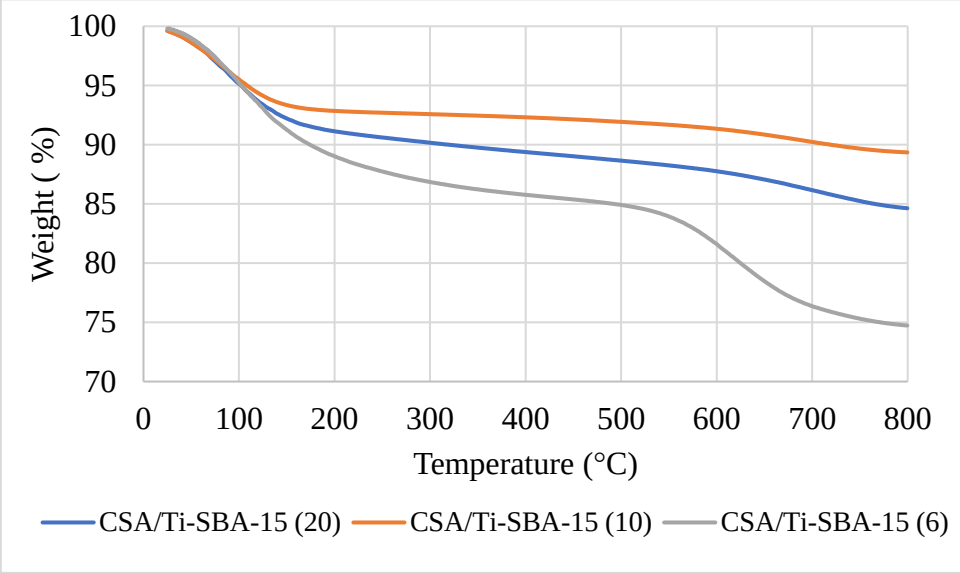

Figure 5.18. TGA results of CSA/Ti-SBA-15 catalysts.

The elemental XRF analysis of the fresh CSA/Ti-SBA-15 catalysts and CSA/SBA-15 were given in Table 5.5. It was observed that CSA/SBA-15 catalyst had the lowest amount of sulfur content (0.143 %). Consequently, Ti incorporation in the catalysts structure was significant for the effect of sulfation, it increased the sulfur content. Compatible with the NH_3-TPD results, higher sulfur content was observed with higher titanium incorporated catalysts.

Table 5.5. Elemental XRF results of the fresh catalysts.

Catalyst	S Content (%)	Ti Content (%)
CSA/SBA-15	0.14	-
CSA/Ti-SBA-15 (6)	1.49	7.79
CSA/Ti-SBA-15 (10)	0.89	5.43
CSA/Ti-SBA-15 (20)	0.33	2.37

5.2. Cellulose Acetate Synthesis

5.2.1. Cellulose Acetylation by H_2SO_4

For comparison purposes, microcrystalline cellulose was homogeneously acetylated according to the study of Biswas et al. (2006) [31] with slight modifications. 0.04 g of H_2SO_4 was used in the reaction as the homogeneous catalyst and the reaction was conducted at 80°C for 4 h [31].

The effect of reaction time on the CA yield and DS was investigated and the results were given in Table 5.6. The results indicated that as the reaction time increased from 1.5 h to 4 h, the cellulose acetate yield also increased from 9.2 % to 36.4 %. Also, almost 43 % of cellulose conversion was obtained in 4 h reaction. DS also increased up to 2.94 in 3 h reaction, indicating the formation of cellulose triacetate (CTA). Decrease in DS was obtained at 4 h reaction time, possibly due to cellulose degradation with prolonged reaction time [10].

Table 5.6. Effect of reaction time on cellulose acetylation with H_2SO_4.

Reaction Time (h)	DS	Yield (%)	Cellulose Conversion (%)
1.5	2.55	9.19	10.78
3.0	2.94	28.81	33.80
4.0	2.39	36.38	42.69

5.2.2. Cellulose Acetylation by Amberlyst-15

The effect of catalyst amount (0.25 g and 0.50 g) on the CA yield and DS are given in Table 5.7 for 6 h reaction. The amount of catalyst was observed to have an impact on the DS and yields of cellulose acetate. A lower amount of Amberlyst-15 (0.25 g) resulted in 58.1 % cellulose acetate yield and almost 70 % cellulose conversion. When the catalyst amount was doubled, around 17 % decrease in the cellulose acetate yield was obtained. Consequently, addition of larger amount of catalyst enhanced the degradation of cellulose acetate, as reported in the literature [11].

Table 5.7. Effect of Amberlyst-15 amount on cellulose acetylation (6 h).

Catalyst amount (g)	DS	Yield (%)	Cellulose Conversion (%)
0.25	2.26	58.10	68.17
0.50	2.31	47.92	56.23

The effect of reaction time on the CA yield and DS was also investigated for 0.25 g Amberlyst-15. As shown Table 5.8, the highest cellulose acetate yield (70 %), cellulose conversion (82.4 %) and DS (2.83) was obtained at shorter reaction time of 3 h. The yield drop with increased reaction time was attributed to the cellulose degradation [10].

Table 5.8. Effect of reaction time on cellulose acetylation with 0.25 g Amberlyst- 15.

Reaction Time (h)	DS	Yield (%)	Cellulose Conversion (%)
3.0	2.83	70.23	82.41
4.5	2.50	60.21	70.65
6.0	2.31	47.92	56.23

5.2.3. Cellulose Acetate Synthesis over SO_4/Ti-SBA-15 Catalyst

The activities of the SO_4/Ti-SBA-15 catalyst was given Table 5.9. However, these catalysts had shown severe sulfur leaching as given in Table 5.10. Therefore, no further studies were performed with these catalysts.

Table 5.9. Reaction results for the SO_4/Ti-SBA-15 (10) catalyst (80 °C, 6 h).

Catalyst Amount (g)	DS	CA Yield (%)	Cellulose Conversion (%)
0.50	2.33	59.10	69.35
0.25	2.22	66.35	77.85

Table 5.10. Sulfur leaching of SO_4/Ti-SBA-15 catalyst.

S Content Before Reaction (ppm)	S Content After Reaction (ppm)	S Leaching (%)
0.560	0.428	23.55

5.2.4. Cellulose Acetate Synthesis over SO_4/TiO_2-SiO_2 and SO_4/La-TiO_2-SiO_2 Catalysts

Activities of SO_4/TiO_2-SiO_2 and SO_4/La-TiO_2-SiO_2 catalysts were given in Table 5.11.

Table 5.11. Reaction results for the leached catalysts (80 °C, 6 h).

Catalyst	Catalyst Amount (g)	DS	CA Yield (%)	Cellulose Conversion (%)
SO_4/TiO_2-SiO_2	0.50	2.53	76.75	90.05
	0.25	2.50	68.90	80.84
SO_4/La-TiO_2-SiO_2	0.50	2.34	54.58	64.05
	0.25	2.35	64.37	75.53

To investigate catalyst stability, the amount of sulfur bound to the surface before and after the cellulose acetylation reaction was analyzed with XRF and compared in Table 5.12. However, serious leaching was observed for thencatalysts. The fact that more sulfate groups were attached to the La-containing SO_4/La-TiO_2-SiO_2 catalyst increased the acidity of the catalyst but caused more sulfur leaching (39.56 %) than the SO_4/TiO_2-SiO_2 catalyst. This leach was probably caused by the weak physical bonds of the sulfate groups to the catalyst surface. Therefore, it was decided that sulfation should be done with a stronger acid to prevent leaching of sulfate groups.

Table 5.12. Sulfur leaching of the SO_4/TiO_2-SiO_2 and SO_4/La-TiO_2-SiO_2 catalysts.

Catalyst	S Content Before Reaction (%)	S Content After Reaction (%)	S Leaching (%)
SO_4/TiO_2-SiO_2	0.449	0.317	29.37
SO_4/La-TiO_2-SiO_2	0.687	0.415	39.56

5.2.5. Cellulose Acetate Synthesis over CSA/Ti-SBA-15 Catalysts

Table 5.13 illustrates the results of cellulose acetylation reaction by CSA/Ti-SBA-15 (10) catalysts for different catalyst amounts at 80 °C for 6 h. The maximum cellulose acetate yield was obtained with 0.25 g catalyst (74.65 %), but the results were very close to each other with 0.10 g catalyst (73.48 %). Maximum cellulose conversion was achieved by 0.25 g of catalyst (87.59 %), followed by 0.1 g catalyst (86.23 %). At the highest catalyst loading (0.5 g), cellulose conversion and cellulose acetate yield decreased. This was related to cellulose acetate breakdown was provided. Degradation of cellulose acetate can proceed with ß-1,4-glycosidic bond disconnection followed by the pyranose ring rupture and acetic acid formation because of partial deacetylation [11].

Table 5.13. Reaction results with CSA/Ti-SBA-15 (10) catalysts (80 °C, 6 h).

Catalyst Amount (g)	DS	Yield (%)	Cellulose Conversion (%)
0.10	2.58	73.48	86.23
0.25	2.69	74.65	87.59
0.50	2.57	65.31	76.63

The influence of reaction time (2 h, 4 h, 6 h, and 8 h) on the CA yield was also examined, which was given in Figure 5.19. Cellulose acetate yield increased with reaction time up to 6 h and it decreased. The decrease in the yield obtained at 8 h reaction was attributed to the degradation of cellulose [10].

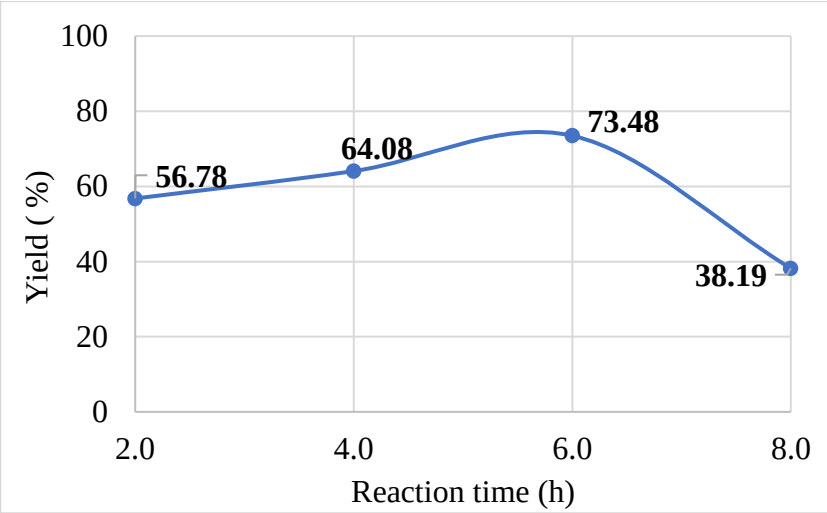

Figure 5.19. Effect of reaction time on cellulose acetylation with 0.1 g CSA/Ti-SBA-15 (10) catalyst.

The reusability of CSA/Ti-SBA-15 (10) catalyst was studied. According to the following results given in Table 5.14, cellulose acetate, yield and cellulose conversion decreased each run. CA yield of approximately 43 % and cellulose conversion of 50 % were obtained after the second catalyst reuse (3rd reaction run).

Table 5.14. Reaction results of 0.25 g CSA/Ti-SBA-15 (10) catalyst (80 °C, 6 h).

Reaction cycle	DS	Yield (%)	Cellulose Conversion (%)
1	2.69	74.65	89.59
2	2.63	67.64	79.37
3	2.55	42.87	50.30

The leaching data of the catalysts was given in Table 5.15. The effect of Ti incorporation on the catalyst stability was examined. Sulfur content of CSA/SBA-15 catalyst after first reaction cycle indicated that only a little amount of the sulfate group was bonded to the surface (0.143 %), but also almost 50 % of the sulfur bound to the catalyst surface had leached due to absence of Ti. CSA/Ti-SBA-15 (6) with the highest amount of Ti was observed to have 1.49 % sulfur content, with 10 % leaching after 1st run. The fact that CSA/Ti-SBA-15 (6) catalyst had both the highest acidity and leaching

can be attributed to the leaching of weakly adsorbed sulfate groups from the catalyst surface during the reaction. As expected, CSA/Ti-SBA-15 (10) and CSA/Ti-SBA-15 (20) catalysts had less sulfur bound to the surface as 0.89 % and 0.33 % and thus lower sulfur leaching as 2.84 % and 5.87 %, respectively. The reason of more sulfur leaching in the CSA/Ti-SBA-15 (20) catalyst than in CSA/Ti-SBA-15 (10) is that it contains more Si in its structure and less S groups attached due to its less molar Ti content. Therefore, due to the weak bonds between the sulfur groups and Si, leaching was observed after the first reaction.

Table 5.15. Catalysts leaching data for cellulose acetylation reaction (80 °C, 6 h).

Catalyst	S Content Before Reaction (%)	S Content After 1st Run (%)	Sulfur Leaching (%)
CSA/SBA-15	0.14	0.07	47.55
CSA/Ti-SBA-15 (6)	1.49	1.36	9.75
CSA/Ti-SBA-15 (10)	0.88	0.86	2.84
CSA/Ti-SBA-15 (20)	0.33	0.30	5.87

After 1 cycle of cellulose acetylation reaction, CSA/Ti-SBA-15 (10) catalyst indicated a high stability and has given the lowest sulfur leaching as 2.84 %. Although the leaching is low, the CA yield was observed to drop significantly in the subsequent reaction runs. Therefore, it was decided to treat the catalyst and examine the leaching and the reaction performance [55].

5.2.5.1. Cellulose Acetylation with Treated CSA/Ti-SBA-15 Catalysts

To increase the reusability of the catalyst, two possibilities were considered. The first one can be the reaction conditions. It was reported in the literature that the polar solvents have an aggressive nature [55]. Acetic anhydride used in the cellulose acetylation is also a polar aggressive solvent, which may have promoted leaching. It was also stated in the literature that higher temperatures are usually detrimental. The literature also suggests that the high or low pH can promote the solubility of surface sulfate groups [55].

In this case, the acidic nature and low pH of acetic anhydride (pH=3) as the reaction medium may have promoted leaching. Considering these 2 possibilities, two treatment methods were considered to increase the reusability of the CSA/Ti-SBA-15 (10) catalyst [55].

As given in Table 5.16, XRF analysis was conducted and the sulfur content after the treatment and after the 1st run were compared to observe the catalyst stability. As the first method, CSA/Ti-SBA-15 (10) catalyst was refluxed with acetic anhydride for 1 h at 80 °C before testing in the reaction. After treatment, it was filtered and dried and named as W-CSA/Ti-SBA-15 (10). It was observed that reflux with acetic anhydride at 80 °C for 1 h led to 12.15 % leaching of sulfur. After W-CSA/Ti-SBA-15 (10) was used in the 1st run, 0.77 % leaching of the catalyst with 75.6 % CA yield and 88.7 % cellulose conversion were obtained. Also, for comparison purposes, W-CSA/Ti-SBA-15 (10) catalyst was washed with deionized water, then filtered and dried. However, significant amount of sulfur leaching was detected after washing (75.93 %), so no reaction was conducted. It was reported in the literature that the reason of catalyst deactivation is the partial solubility of the active species in water [56].

Table 5.16. XRF results of the treated CSA/Ti-SBA-15 (10) catalysts.

Catalyst	S Content After Treatment (%)	S Leaching (%)	S Content After 1st Run (%)	S Leaching (%)
W-CSA/Ti-SBA-15 (10) *	0.78	12.15	0.775	0.77
WW-CSA/Ti-SBA-15 (10) **	0.21	75.93	N.D.	N.D.

* Refluxed with acetic anhydride (80 °C, 1 h).
** Refluxed with acetic anhydride (80 °C, 1 h), then washed with deionized water.

To further investigate sulfur leaching, CSA/Ti-SBA-15 (10) catalyst was used directly in the reaction and then refluxed with acetone for 0.5 h after, filtered, and dried. The sulfur content after the reaction was observed as 0.77 % which showed 13.21 % leaching, as given in Table 5.17.

Table 5.17. XRF results of the treated CSA/Ti-SBA-15 (10) catalysts.

Catalyst	S Content Before Reaction (%)	S Content After 1st Run and Acetone Reflux (%)	S Leaching (%)
A-CSA/Ti-SBA-15 (10) ***	0.889	0.772	13.21

*** Refluxed with acetone (60°C, 0.5 h) after the reaction.

Consequently, both treated catalysts A-CSA/Ti-SBA-15 (10) and W-CSA/Ti-SBA-15 (10) catalysts had close sulfur contents 1st run as 0.772 % and 0.775 %, respectively. The reusability of A-CSA/Ti-SBA-15 (10) was studied for 3 reaction runs.

The CA yield, DS, and cellulose conversion were given in Table 5.18. The purpose of acetone treatment between each cycle was to remove any weakly bound leached sulfur from the surface to increase the reusability of the catalyst and to prevent the catalyst pore plugging event. In the first cycle, 73.1 % CA yield with 2.7 DS and 85.8 % cellulose conversion were obtained. At the end of the 3rd reaction cycle, 50 % CA yield with 2.62 DS and 58.6 % cellulose conversion were observed.

Table 5.18. Reaction results of A-CSA/Ti-SBA-15 (10) (80 °C, 6 h, 0.1 g catalyst, 1 g MCC, nAA/nAGU= 10:1).

Reaction cycle	DS	CA Yield (%)	Cellulose Conversion (%)
1	2.70	73.10	85.80
2	2.69	64.61	75.81
3	2.62	49.99	58.66

The sulfur content of the catalysts was analyzed by XRF and was given in Table 5.19. At the end of 3rd run, 1.68 % sulfur leaching was observed.

Table 5.19. Sulfur leaching data of A-CSA/Ti-SBA-15 (10) after 3rd run.

Run	S Content (%)	S Leaching (%)
3rd Run	0.76	1.68

The mass balance of the three reaction cycles were given in Table 5.20. For each reaction, the cellulose mass balance was established for MCC, CA, and CTA. Since the mass is conserved, the cellulose amount in the products (CA and CTA) was subtracted from the reactant (MCC) and the remained amount of cellulose has been degraded during the reaction. As mentioned earlier, cellulose degradation takes place by the ß-1,4-glycosidic bond disconnection between AGU units [11].

Table 5.20. Mass balance of the cellulose acetylation reaction.

	MCC (g)	CA (g)	CTA (g)	Degraded cellulose (g)
1st reaction	1.00	1.31	$9x10^{-2}$	
Cellulose Amount (g)	1.00	0.86	$5\ x10^{-2}$	0.09
2nd reaction	1.00	1.16	$7.5\ x10^{-2}$	
Cellulose Amount (g)	1.00	0.76	$4\ x10^{-2}$	0.20
3rd reaction	1.00	0.90	$8\ x10^{-3}$	
Cellulose Amount (g)	1.00	0.58	$4\ x10^{-3}$	0.41

FT-IR spectrum of cellulose acetate was given in Figure 5.20. The spectroscopy result displays clear evidence of acetylation with three ester bond peaks. The observed ester bond peaks are as follows: carbonyl C=O stretching of ester at 1738 cm^{-1}, C-H stretching in $–O(C=O)-CH_3$ at 1368 cm^{-1}, and C-O stretching of acetyl group at 1214 cm^{-1}. The absence of O-H stretching vibrations observed in MCC also suggests the successful substitution of hydroxyl groups in the cellulose with the acetyl groups. Furthermore, the absence of a peaks in the range of 1840-1760 cm^{-1} and 1700 cm^{-1} indicated that the product was both free of byproducts unreacted acetic anhydride and acetic acid [18].

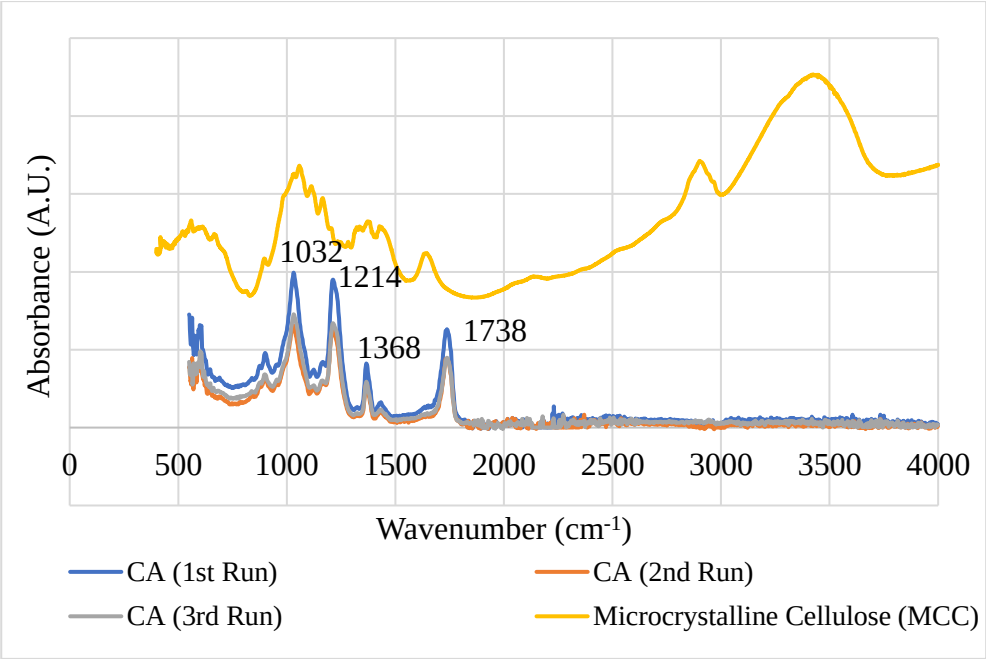

Figure 5.20. FT-IR spectroscopy of MCC and cellulose acetate samples (1st, 2nd and 3rd run samples).

The influence of structural modifications on degradation behavior was investigated using thermo gravimetric analysis (TGA) on microcrystalline cellulose and cellulose acetate and was given in Figure 5.21. From 50 ^{o}C to 250 ^{o}C, the weight loss was associated with vaporization of physically adsorbed water. Microcrystalline cellulose showed constant weight loss in this temperature range, but cellulose acetate showed progressive degradation due to its hydrophobic nature [57]. At temperatures above 250 °C, CA had rapid pyrolysis resulted in char, tar, and volatile compounds production [1]. Fast pyrolysis was observed in the temperature range of 250–450 ^{o}C, as shown by the TGA plot [57]. In general, it was shown that acetylated cellulose had greater thermal stability than untreated cellulose. This demonstrated that acetylation had little impact on the thermal stability of cellulosic materials [18].

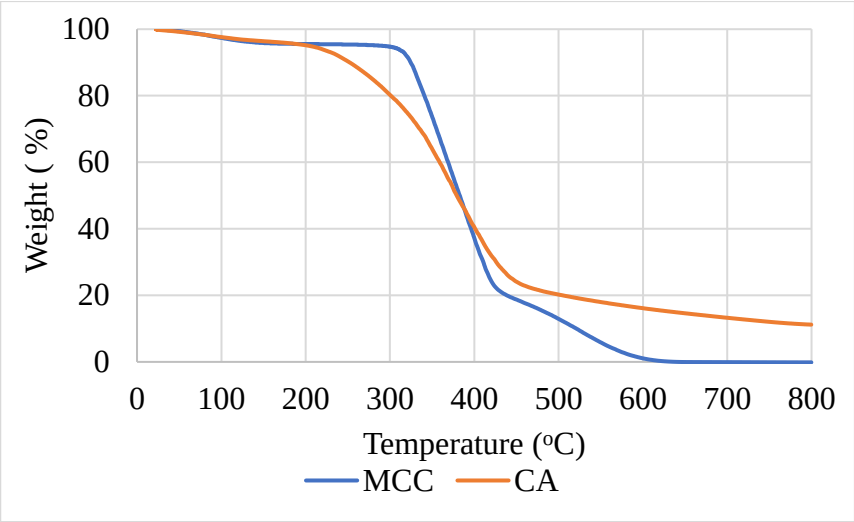

Figure 5.21. TGA results of MCC and CA sample.

Figure 5.22 illustrates the ^{1}H-NMR spectroscopy of cellulose acetate sample synthesized with A-CSA/Ti-SBA-15 (10) catalyst. In the CA sample, the characteristic acetate signals (-CH_3) and cellulose AGU unit signals (-CH) between 1.8–2.1 ppm and 3.5–5.0 ppm, were observed respectively.

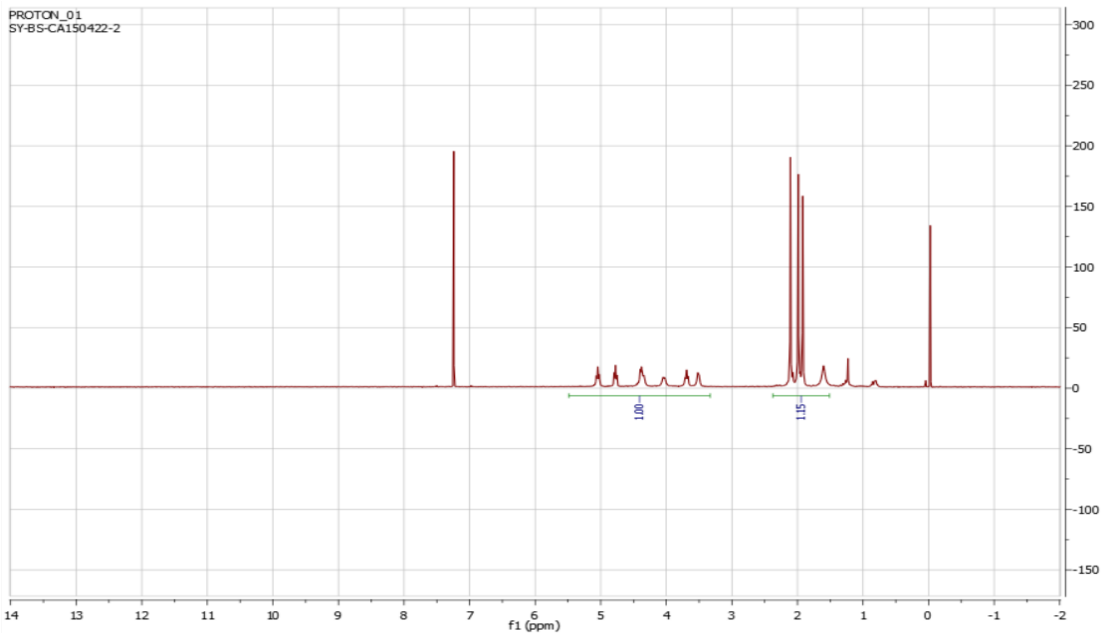

Figure 5.22. ^{1}H-NMR spectroscopy of cellulose acetate sample (80 °C, 6 h, 0.1 g of A-CSA/Ti-SBA-15 (10), 1 g MCC, nAA/nAGU= 10:1).

CHAPTER 6

CONCLUSION

Mesoporous and acidic SO_4/Ti-SBA-15, SO_4/La-TiO_2-SiO_2, SO_4/TiO_2-SiO_2 catalysts with high BET surface areas (440-647 m^2/g) were prepared using ammonium sulfate as sulfating agent. Also, chlorosulfonic acid sulfated mesoporous catalysts CSA/Ti-SBA-15 with different titanium content (Si/Ti mol ratios of 6 to 20) and high surface area (398-1028 m^2/g) were synthesized. Sulfation decreased catalyst surface area and pores sizes which was attributed the linkage of sulfate groups to the catalyst surface. The sulfur content the acidity of the catalysts was enhanced with lanthanum and titanium incorporation and chlorosulfonic acid treatment.

The catalyst prepared by ammonium sulfation showed significant leaching in cellulose acetylation. CSA/Ti-SBA-15 (10) was found as the most stable and active catalyst with 2.84 % sulfate group leaching. It provided 89.6 % cellulose conversion with 74.6 % CA yield and DS of 2.69. At prolonged reaction times (8 h) and increased catalyst amount (0.5 g) the yield decreases were related to cellulose and CA degradation, respectively. Significant sulfur leaching was detected (75.93 %) after treating CSA/Ti-SBA-15 (10) catalyst with deionized water.

In order to remove loosely bound sulfur from the surface and to prevent the catalyst pore plugging event, acetone treatment after each reaction cycle was employed. In the 1st reaction cycle, A-CSA/SBA-15 (10) provided 86 % conversion, 73 % CA yield, and DS of 2.7. The 3rd reuse of the A-CSA/Ti-SBA-15 (10) indicated that acetone treatment yielded 58.6 % conversion, 50 % of yield, and DS of 2.62. Consequently, at the end of 3rd reaction cycle, a highly active and stable catalyst with 1.68 % sulfur leaching was reported.

REFERENCES

[1] D.N.-S. Hon, Cellulose: Chemistry and Technology, *Encyclopedia of Materials: Science and Technology*, 2001, 1039-1045.

[2] Abdel-Halim, E. S., Chemical modification of cellulose extracted from sugarcane bagasse: Preparation of Hydroxyethyl Cellulose, *Arabian Journal of Chemistry*, 2014, 7(3), 362-371.

[3] Sharma, R., Varshney, V. K., Chauhan, G. S., Naithani, S., & Soni, P. L., Hydroxypropylation of Cellulose Isolated From Bamboo (Dendrocalamus Strictus) Concerning Hydroxypropyl Content and Rheological Behavior of the Hydroxypropyl Cellulose, *Journal of Applied Polymer Science*, 2009, 113(4), 2450-2455.

[4] Dai, L., Zhao, Q., Fang, M., Liu, R., Dong, M., & Jiang, T., Catalytic activity comparison of Zr–SBA-15 immobilized by a Brønsted–Lewis acidic ionic liquid in different esterifications, *RSC Advances*, 2017, 7(51), 32427-32435.

[5] Meiland, M., Liebert, T., & Heinze, T., Tailoring the Degree of Polymerization of Low Molecular Weight Cellulose, *Macromolecular Materials and Engineering*, 2011, 296(9), 802.

[6] Kuo, C.M., Bogan, R.T., Process for the Manufacture of Cellulose Acetate. *U.S. Patent*, 1997, 5,608,050.

[7] Steinmeier, H., Acetate Manufacturing, Process and Technology, *WILEY-VCH Verlag*, 2004, 208(1), 49-60.

[8] Heinze, T., & Liebert, T., Unconventional Methods in Cellulose Functionalization, *Progress in Polymer Science*, 2001, 26(9), 1689-1762.

[9] Yan, L., Li, W., Qi, Z., & Liu, S., Solvent-Free Synthesis of Cellulose Acetate By Solid Superacid Catalysis, *Journal of Polymer Research*, 2006, 13(5), 375-378.

[10] Fan, G., Wang, M., Liao, C., Fang, T., Li, J., & Zhou, R., Isolation of Cellulose from Rice Straw and Its Conversion into Cellulose Acetate Catalyzed by Phosphotungstic Acid, *Carbohydrate Polymers*, 2013, 94(1), 71-76.

[11] Fan, G., Liao, C., Fang, T., Luo, S., & Song, G., Amberlyst 15 as a New and Reusable Catalyst for the Conversion of Cellulose into Cellulose Acetate, *Carbohydrate Polymers*, 2014, 112, 203-209.

[12] Pinkert, A., Marsh, K. N., Pang, S., & Staiger, M. P. (2009). Ionic Liquids and Their Interaction with Cellulose. *Chemical Reviews*, 109(12), 6712-6728.

[13] Konwar, L. J., Mäki-Arvela, P., Thakur, A. J., Kumar, N., & Mikkola, J. P., Sulfonated Carbon as a New, Reusable Heterogeneous Catalyst for One-Pot Synthesis of Acetone Soluble Cellulose Acetate, *RSC Advances*, 2016, 6(11), 8829-8837.

[14] Zhao, D., Feng, J., Huo, Q., Melosh, N., Fredrickson, G. H., Chmelka, B. F., & Stucky, G. D., Triblock Copolymer Syntheses of Mesoporous Silica with Periodic 50 To 300-Angstrom Pores, *Science*, 1998, 279(5350), 548-552.

[15] Zhao, D., Sun, J., Li, Q., & Stucky, G. D., Morphological Control of Highly Ordered Mesoporous Silica SBA-15, *Chemistry of Materials*, 2000, 12(2), 275-279.

[16] Zhao, Q., Yang, C., Fang, M., & Jiang, T., Performance of Brønsted-Lewis Acidic Ionic Liquids Supported Ti-SBA-15 for the Esterification of Acetic Acid to Benzyl Alcohol, *Applied Catalysis A: General*, 2020, 594, 117470.

[17] Li, J.-Z., Furuno, T., Katoh, S., & Uehara, T., Chemical Modification of Wood by Anhydrides Without Solvents or Catalysts, *Journal of Wood Science*, 2000, 46(3), 215–221.

[18] Li, J., Zhang, L. P., Peng, F., Bian, J., Yuan, T. Q., Xu, F., & Sun, R. C., Microwave-Assisted Solvent-Free Acetylation of Cellulose with Acetic Anhydride in the Presence of Iodine as a Catalyst, *Molecules*, 2009, 14(9), 3551-3566.

[19] Adinugraha, M. P., & Marseno, D. W., Synthesis and Characterization Of Sodium Carboxymethylcellulose from Cavendish Banana Pseudostem (Musa Cavendishii Lambert), *Carbohydrate Polymers*, 2005, 62(2), 164-169.

[20] Daicel.com. 2022. Features of Cellulose Acetate | Daicel corporation. [online] Available at: <https://www.daicel.com/cell_ac/en/cellulose/> [Accessed 23 February 2022].

[21] Sigmaaldrich.com. 2022. Cellulose acetate - Acetylcellulose. [online] Available at: <https://www.sigmaaldrich.com/TR/en/substance/celluloseacetate123459004357> [Accessed 23 February 2022].

[22] McGath, M., Jordan-Mowery, S., Pollei, M., Heslip, S., & Baty, J., Cellulose Acetate Lamination: A Literature Review and Survey of Paper-Based Collections in the United States, *International Journal for the Preservation of Library and Archival Material*, 2015, 36(4).

[23] Gent, A. N., Kauffman, George B., Rodriguez, Ferdinand, Preston, J., Stevens, Malcolm P. and Bierwagen, Gordon P., Major Industrial Polymers, *Encyclopedia Britannica*, 2016.

[24] Daicel.com. 2022. Technical information about cellulose acetate | Daicel corporation. [online] Available at: <https://www.daicel.com/cell_ac/en/detail/> [Accessed 23 February 2022].

[25] Zionmarketresearch.com. 2021. Global Cellulose Acetate Market to Witness Impressive Growth, Revenue to Surge to USD 10.25 Billion By 2028. [online] Available at: <https://www.zionmarketresearch.com/news/global-cellulose-acetate-market> [Accessed 23 February 2022].

[26] Zionmarketresearch.com. 2021. Cellulose Acetate Market- Global Industry Perspective, Comprehensive Analysis and Forecast, 2021 – 2028. [online] Available at: <https://www.zionmarketresearch.com/report/cellulose-acetate-market> [Accessed 23 February 2022].

[27] Zhang, X., Zhang, W., Tian, D., Zhou, Z., & Lu, C., A New Application of Ionic Liquids for Heterogeneously Catalyzed Acetylation of Cellulose Under Solvent-Free Conditions, *RSC Advances*, 2013, 3(21), 7722-7725.

[28] Wolfs, J., & Meier, M. A., A More Sustainable Synthesis Approach for Cellulose Acetate Using the DBU/CO_2 Switchable Solvent System, *Green Chemistry*, 2021, 23(12), 4410-4420.

[29] Lopes, J. M., Bermejo, M. D., Martín, Á., & Cocero, M. J., Ionic Liquid as Reaction Media for the Production of Cellulose-Derived Polymers from Cellulosic Biomass, *ChemEngineering*, 2017, 1(2), 10.

[30] Heinze, T., Schwikal, K., & Barthel, S., Ionic Liquids as Reaction Medium in Cellulose Functionalization, *Macromolecular Bioscience*, 2005, 5(6), 520-525.

[31] Biswas, A., Saha, B. C., Lawton, J. W., Shogren, R. L., & Willett, J. L., Process for Obtaining Cellulose Acetate from Agricultural By-Products, *Carbohydrate Polymers*, 2006, 64(1), 134-137.

[32] Gericke, M., Fardim, P., & Heinze, T., Ionic liquids—Promising but Challenging Solvents for Homogeneous Derivatization of Cellulose, *Molecules*, 2012, 17(6), 7458-7502.

[33] Meng, C., Cao, G. P., Li, X. K., Yan, Y. Z., Zhao, E. Y., Hou, L. Y., & Shi, H. Y., Structure of the SO_4^{2-}/TiO_2 Solid Acid Catalyst and its Catalytic Activity in Cellulose Acetylation, *Reaction Kinetics, Mechanisms, and Catalysis*, 2017, 121(2), 719-734.

[34] Puls, J., Wilson, S. A., & Hölter, D., Degradation of Cellulose Acetate-Based Materials: A Review, *Journal of Polymers and the Environment*, 2011, 19(1), 152-165.

[35] Chen, Y., Huang, Z., Yang, J., Zhu, W., Mo, J., & Liu, L, Preparation Technology of Cellulose Acetate from Sugarcane Bagasse by Mechanical Activation, *Transactions of the Chinese Society of Agricultural Engineering*, 2010, 26(9), 374-380.

[36] Kruk, M., Jaroniec, M., Ko, C. H., & Ryoo, R. Characterization of the porous structure of SBA-15, *Chemistry of Materials*, 2000, 12(7), 1961-1968.

[37] Beck, J. S., Vartuli, J. C., Roth, W. J., Leonowicz, M. E., Kresge, C. T., Schmitt, K. D., & Schlenker, J., A New Family of Mesoporous Molecular Sieves Prepared with Liquid Crystal Templates, *Journal of the American Chemical Society*, 1992, 114(27), 10834-10843.

[38] Zhao, D., Huo, Q., Feng, J., Chmelka, B. F., & Stucky, G. D., Nonionic Triblock and Star Diblock Copolymer and Oligomeric Surfactant Syntheses of Highly Ordered, Hydrothermally Stable, Mesoporous Silica Structures, *Journal of the American Chemical Society*, 1998, 120(24), 6024-6036.

[39] Mutlu, V. N., & Yilmaz, S., Esterification of Cetyl Alcohol with Palmitic Acid over WO_3/Zr-SBA-15 and Zr-SBA-15 Catalysts, *Applied Catalysis A: General*, 2016, 522, 194-200.

[40] Chaudhary, V., & Sharma, S., An Overview of Ordered Mesoporous Material SBA-15: Synthesis, Functionalization, and Application in Oxidation Reactions, *Journal of Porous Materials*, 2017, 24(3), 741-749.

[41] Sharma, R. V., & Dalai, A. K., Synthesis of Bio-Lubricant From Epoxy Canola Oil Using Sulfated Ti-SBA-15 Catalyst, *Applied Catalysis B: Environmental*, 2013, 142, 604-614.

[42] Yadav, G. D., & Murkute, A. D., Preparation of a Novel Catalyst Udcat-5: Enhancement in Activity of Acid-Treated Zirconia—Effect Of Treatment With Chlorosulfonic Acid Vis-À-Vis Sulfuric Acid, *Journal of Catalysis*, 2004, 224(1), 218-223.

[43] Rashid, R., Afroze, F., Ahmed, S., Miran, M. S., Bin, A., & Susan, H., Control of the Porosity and Morphology of Ordered Mesoporous Silica by Varying Calcination Conditions, *Materials Today: Proceedings*, 2019, 15, 546-554.

[44] Li, L., Liu S., Xu J., Yu S., Liu F., Xie C., Ge X., Ren J., Esterification of Itaconic Acid Using Ln-SO_4^{2-}/Tio_2–Sio_2 (Ln = La^{3+}, Ce^{4+}, Sm^{3+}) as Catalysts, *Journal of Molecular Catalysis A: Chemical*, 2013, 368, 24-30.

[45] Shao G. N., Sheikh R., Hilonga A., Lee J. E., Park Y. H., Kim H. T., Biodiesel Production by Sulfated Mesoporous Titania–Silica Catalysts Synthesized by the Sol-Gel Process from Less Expensive Precursors, *Chemical Engineering Journal*, 2013, 215-216, 600–607.

[46] Sharma, R. V., Soni, K. K., & Dalai, A. K., Preparation, Characterization, and Application of Sulfated Ti-SBA-15 Catalyst for Oxidation of Benzyl Alcohol to Benzaldehyde, *Catalysis Communications*, 2012, 29, 87-91.

[47] Yang, H., Lu, R., Zhao, J., Yang, X., Shen, L., Wang, Z., Sulfated Binary Oxide Solid Superacids, *Materials Chemistry and Physics*, 2003, 80, 68-72.

[48] Sun, X., Lu, C., Zhang, W., Tian, D., & Zhang, X., Acetone-Soluble Cellulose Acetate Extracted from Waste Blended Fabrics via Ionic Liquid Catalyzed Acetylation, *Carbohydrate Polymers*, 2013, 98(1), 405-411.

[49] Zhang, X., Zhang, W., Tian, D., Zhou, Z., & Lu, C., A New Application of Ionic Liquids for Heterogeneously Catalyzed Acetylation of Cellulose Under Solvent-Free Conditions, *RSC Advances*, 2013, 3(21), 7722-7725.

[50] Asghari, F. S., Yoshida, H., Dehydration of Fructose To 5- Hydroxymethylfurfural in Subcritical Water Over Heterogeneous Zirconium Phosphate Catalysts, *Carbohydrate Research*, 2006, 341, 2379-2387.

[51] Shields, J.E., Lowell, S., Thomas, M.A., Thommes, M. Characterization of Porous Solids and Powders: Surface Area, Pore Size and Density, *Kluwer Academic Publisher: Boston*, 2004, 43–45.

[52] Ren, J., Li, Z., Liu, S., Xing, Y., & Xie, K., Silica–Titania Mixed Oxides: Si–O–Ti Connectivity, Coordination of Titanium, and Surface Acidic Properties, *Catalysis Letters*, 2008, 124(3), 185-194.

[53] Radha, A. V., Lander, L., Rousse, G., Tarascon, J. M., & Navrotsky, A., Thermodynamic Stability and Correlation with Synthesis Conditions, Structure and Phase Transformations in Orthorhombic and Monoclinic $Li_2M(SO_4)_2$ (M= Mn, Fe, Co, Ni) Polymorphs, *Journal of Materials Chemistry A*, 2015, 3(6), 2601-2608.

[54] Zhang, X., Huang, Y., Guo, Y., Yuan, X., & Jiao, F., Catalytic Performance of Surface-Silylated and Phenyl-Bridged Ti-Containing Mesoporous Silica for Epoxidation of Propylene, *Microporous and Mesoporous Materials*, 2018, 262, 251-257.

[55] Sadaba, I., Granados, M. L., Riisager, A., & Taarning, E., Deactivation of Solid Catalysts in Liquid Media: The Case of Leaching of Active Sites in Biomass Conversion Reactions, *Green Chemistry*, 2015, 17(8), 4133-4145.

[56] Okuhara, T., Water-Tolerant Solid Acid Catalysts, *Chemical Reviews*, 2002, 102(10), 3641-3666.

[57] Yeng, L. C., Wahit, M. U., & Othman, N., Thermal and Flexural Properties of Regenerated Cellulose (RC)/Poly (3-Hydroxybutyrate) (PHB) Biocomposites, *Jurnal Teknologi*, 2015, 75(11).

[58] Berteau, P., & Delmon, B., Modified Aluminas: Relationship Between Activity in 1-Butanol Dehydration and Acidity Measured by NH_3 TPD, *Catalysis Today*, 1989, 5(2), 121-137.